I&EC research
Industrial & Engineering Chemistry Research
pubs.acs.org/IECR
Article

Magnesium Ferrite/Poly(cysteine methacrylate) Nanocomposites for pH-Tunable Selective Removal and Enhanced Adsorption of Indigo Carmine and Methylene Blue

Tanapong Kunakham, Supawitch Hoijang, Minh Dang Nguyen, Supon Ananta, T. Randall Lee, and Laongnuan Srisombat*

Cite This: *Ind. Eng. Chem. Res.* 2022, 61, 18744−18761

Read Online

ACCESS | Metrics & More | Article Recommendations | Supporting Information

ABSTRACT: Magnesium ferrite ($MgFe_2O_4$) and silica-coated $MgFe_2O_4$ nanoparticles were grafted with poly(cysteine methacrylate) (i.e., $MgFe_2O_4$/PCysMA and $MgFe_2O_4$@SiO_2/PCysMA nanocomposites) to study pH-tunable adsorption and enhanced capacities for the adsorption of anionic indigo carmine (IC) and cationic methylene blue (MB) dyes. Several characterization techniques (i.e., XRD, FTIR, TGA, ζ potential analysis, VSM, FE-SEM, TEM, N_2 adsorption−desorption isotherm, and XPS) indicated successful syntheses of these nanocomposites. The adsorption behaviors of the dyes demonstrated that the PCysMA-modified nanoadsorbents could selectively adsorb either IC or MB from either single-component or binary dye systems if the initial pH of the dye solution was tailored appropriately (i.e., pH ∼2 for IC and pH ∼10 for MB). The selective adsorption of these dyes was proposed by the electrostatic attractions of the nanoadsorbents and the dyes. Adsorption isotherms also showed enhanced capacities of $MgFe_2O_4$ and $MgFe_2O_4$@SiO_2 NPs for the adsorption of IC and MB after grafting with PCysMA. Interestingly, the $MgFe_2O_4$@SiO_2/PCysMA nanoadsorbent provided highly pH-selective adsorption and large increases in the capacities for the adsorption of IC and MB, which were attributed to the amounts of PCysMA grafted onto different magnetic substrates. The coating of silica on the surfaces of magnetic nanoparticles provided a higher amount of 3-methacryloxypropyltrimethoxysilane, promoting the polymerization of CysMA monomer. Recycling tests indicated that high efficiencies (∼80%) for the adsorption of IC and MB by the PCysMA-modified nanoadsorbents were obtained after five adsorption−desorption cycles. These key findings showed that the $MgFe_2O_4$/PCysMA and $MgFe_2O_4$@SiO_2/PCysMA nanocomposites exhibited excellent pH-tunable adsorption of anionic and cationic dyes, easy magnetic separation, good reusability, and high stability. Specifically, the $MgFe_2O_4$@SiO_2/PCysMA nanocomposite offers highly pH-selective adsorption and high adsorption capacities for dyes, demonstrating promising and alternative nanoadsorbents for applications in wastewater treatment and sensors.

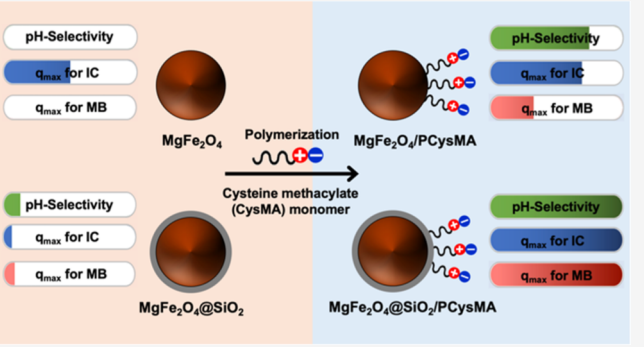

1. INTRODUCTION

Water pollution remains a serious concern due to the rapid growth of industries and technologies.[1,2] Discharge of organic dyes into water resources has greatly affected the ecosystem and organisms since these dyes are toxic, carcinogenic, and nonbiodegradable.[3,4] Therefore, it is urgent to remove contaminated dyes from wastewater before discharging them to natural water resources. Among several treatment methods, adsorption is one of the most attractive methods for removing dyes owing to its ease of operation and high efficiency; the adsorbents used do not generate secondary pollutants, and many are readily available.[5,6] Ideally, an efficient adsorbent exhibits high adsorption capacity, simplicity of adsorbent separation, high recyclability, and high selectivity.[7,8] In particular, an adsorbent with high specificity for binding targeted molecules can be applied to separate/recover, identify, and quantify the targeted dye from environmental and food samples.[9,10] Although numerous adsorbents have been developed to achieve selective adsorption of dyes, most of these exhibit selective adsorption for only one type of dye (i.e., cationic or anionic).[11−15] For example, Jiang et al.[11] reported that a β-cyclodextrin-based polymer provided selective adsorption of an anionic dye (methyl orange, MO) from a mixture of anionic MO and a cationic dye (methylene blue,

Received: September 5, 2022
Revised: November 24, 2022
Accepted: December 2, 2022
Published: December 16, 2022

MB). In contrast, Mantasha et al.[12] demonstrated that a copper-based metal-organic framework (MOF) provided highly selective adsorption of cationic MB over anionic MO in a binary solution of MB/MO. Likewise, Liu et al.[13] reported that nanofibrous membranes selectively adsorbed cationic MB from a MB/MO solution. In these studies, selective adsorption of dyes occurred via electrostatic interactions attributed to specific functional groups of adsorbents and adsorbates. The β-cyclodextrin-based polymer has positively charged ammonium groups, which facilitate the adsorption of anionic dyes. Cu-based MOFs and nanofibrous membranes contain negatively charged carboxyl groups that provide strong interactions with cationic dyes. The studies indicate that a specific functional group on an adsorbent is one of the most important factors for realizing selective adsorption. To extend the capability of adsorbents, it is very necessary to develop adsorbents exhibiting selective adsorption of both cationic and anionic dyes.[2,4,16] Liu et al.[2] reported a polymeric adsorbent, poly(dimethylaminoethyl methacrylate) crosslinked with phytic acid (i.e., PAGD), a pH-dependent adsorbent for selective adsorption of anionic reactive red 24 and cationic fuchsin basic dyes at pH 3 and pH 9, respectively. Similarly, Fan et al.[4] reported that polyacrylonitrile fibers treated hydrothermally with hyperbranched polyethyleneimine (PANF-*g*-HPEI) selectively adsorbed either anionic MO or cationic MB when solution pH was tailored appropriately (i.e., pH 3 for MO and pH 10 for MB). Selective adsorption of anionic and cationic dyes by the PAGD and PANF-*g*-HPEI adsorbents was driven by electrostatic interactions corresponding to the bifunctional groups of the polymers. The bifunctional groups are composed of two specific functional groups and can exist as cations, anions, or zwitterions, depending on the pH of the solution.[17] According to these studies, polymeric adsorbents containing zwitterions were promising adsorbents for pH-dependent adsorption of anionic and cationic dyes. In addition, these adsorbents provided high adsorption capacities and good biocompatibility.[16,18] However, separation of the polymeric adsorbents after the adsorption process required conventional techniques (e.g., centrifugation and filtration), which are tedious methods and limit scaled-up applications.[19,20] Interestingly, poly(cysteine methacrylate) (PCysMA), one of the most attractive zwitterionic polymers, can be simply synthesized by radical polymerization of monomeric cysteine methacrylate (CysMA). The chemical structure of PCysMA is shown in Scheme 1. Likewise, the

Scheme 1. Chemical Structure of Poly(cysteine methacrylate)

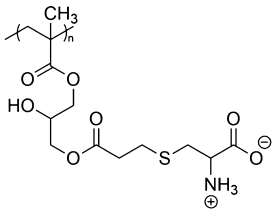

CysMA monomer can be simply prepared from cysteine and methacrylate precursors by using a one-pot thiol-Michael addition reaction in an aqueous medium.[21] In addition to its biocompatibility and availability, cysteine is an amino acid containing bifunctional groups, including amine and carboxyl groups.[22] Importantly, these groups can be either positively or negatively charged by tuning the pH of the solution, which facilitates the adsorption of both anionic and cationic dyes (see Scheme 1). However, PCysMA is readily soluble in water, leading to its limited application as an adsorbent in aqueous solutions.[23] Thus, the preparation of a composite comprising the polymer and other materials (i.e., substrates) is considered a better choice for overcoming solubility limitations. Among several materials, magnetic nanoparticles have been selected as substrates for the fabrication of composites since the magnetic materials exhibit rapid and simple separation of adsorbents with an external magnet.[24] Previously, magnesium ferrite nanoparticles ($MgFe_2O_4$ NPs) were reported to be efficient magnetic nanomaterials due to their superparamagnetic behavior and high saturation magnetization, which contributed to their easy separation from the treated medium with a permanent magnet.[25] In addition to the simple synthesis by a one-pot co-precipitation method, $MgFe_2O_4$ NPs are non-cytotoxic materials that offer environmental safety and practical utility.[26] Preparation of magnetic nanocomposites composed of magnetic nanoparticles and PCysMA can be realized via a radical polymerization reaction. The reaction requires free vinyl (C═C) groups of the magnetic nanoparticles to polymerize with the CysMA monomer.[27] Thus, the surfaces of $MgFe_2O_4$ NPs must be attached to vinyl groups before polymerization with the CysMA monomer. According to the literature, the surfaces of pristine and silica-coated magnetic nanoparticles (i.e., Fe_3O_4 and Fe_3O_4@SiO_2 NPs) can be successfully functionalized with 3-methacryloxypropyltrimethoxysilane (i.e., MPS) to attach C═C groups for further polymerization.[28,29] However, surface modification of different magnetic nanoparticles by MPS and the effects of the resulting materials on polymerization with the CysMA monomer and adsorption of anionic and cationic dyes have not been examined. Therefore, in this study, $MgFe_2O_4$ and $MgFe_2O_4$@SiO_2 NPs were chosen as substrates to investigate the effects of silica surfaces on the selective adsorption of the dyes. To the best of our knowledge, magnetic nanocomposites (i.e., $MgFe_2O_4$/PCysMA and $MgFe_2O_4$@SiO_2/PCysMA) are expected to be alternative nanoadsorbents for pH-selective removal of both anionic and cationic dyes. Additionally, there is no previous report on the utilization of these nanocomposites as pH-selective nanoadsorbents for dyes.

This study focused on the syntheses of $MgFe_2O_4$/PCysMA and $MgFe_2O_4$@SiO_2/PCysMA nanocomposites for use as pH-selective adsorbents in dye removal. The magnetic nanoparticles were used as supports, facilitating the separation purpose. PCysMA with bifunctional groups provided active sites to binding with the target dyes. SiO_2 component in the latter nanocomposite, which severed as a modifier, enhanced the polymerization of the CysMA monomer. The preparation of the magnetic nanocomposites via radical polymerization comprised two steps. First, the surfaces of $MgFe_2O_4$ and $MgFe_2O_4$@SiO_2 NPs were functionalized with MPS to obtain vinyl (C═C) groups on the surfaces of the magnetic nanoparticles. Then, polymerization of the CysMA monomer on the surfaces of the magnetic-based nanoparticles was performed. The as-obtained nanocomposites were fully characterized by several techniques. The effects of initial dye solution pH on the adsorption of anionic and cationic dyes by pristine and composite nanoadsorbents were examined. Indigo carmine (IC) and methylene blue (MB) were used as the representative anionic and cationic dyes, respectively. Then, pH-selective adsorption of various dyes (i.e., IC, MB,

https://doi.org/10.1021/acs.iecr.2c03206
Ind. Eng. Chem. Res. 2022, 61, 18744−18761

Scheme 2. Syntheses of $MgFe_2O_4$/PCysMA and $MgFe_2O_4$@SiO_2/PCysMA Nanocomposites

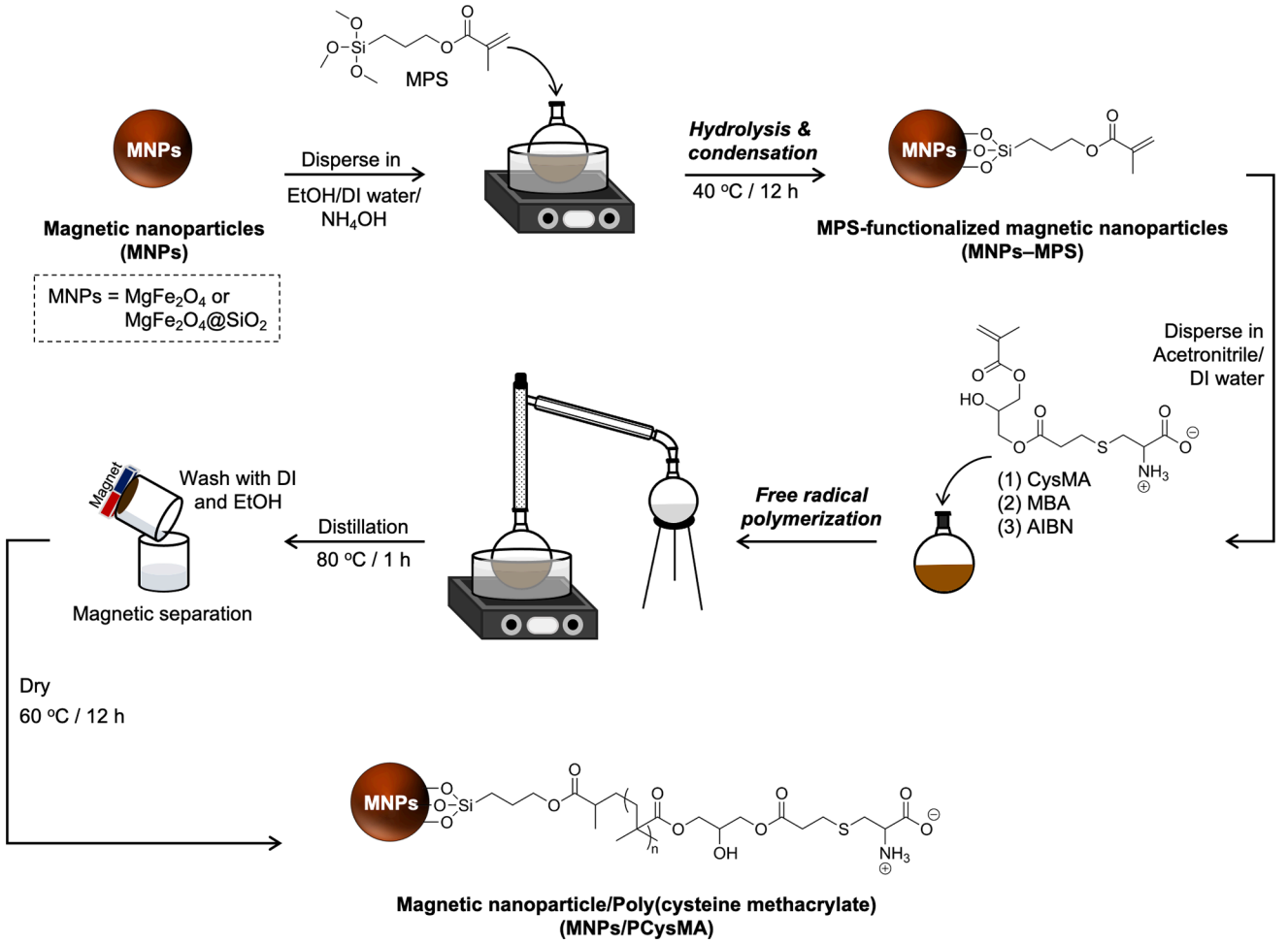

rhodamine B, and methyl orange) from both single-component and binary dye solutions was investigated. Adsorption isotherms of the $MgFe_2O_4$/PCysMA and $MgFe_2O_4$@SiO_2/PCysMA nanocomposites for the adsorption of IC and MB were also obtained to determine the maximum adsorption capacities for these dyes. To demonstrate the reusability of the $MgFe_2O_4$/PCysMA and $MgFe_2O_4$@SiO_2/PCysMA nanocomposites, adsorption−desorption experiments were also performed and evaluated.

2. EXPERIMENTAL SECTION

2.1. Materials. Magnesium ferrite nanoparticles ($MgFe_2O_4$ NPs) with ∼90 nm of particle size and silica-coated magnesium ferrite nanoparticles ($MgFe_2O_4$@SiO_2 NPs) with ∼120 nm of particle size were synthesized as in our previous work.[30,31] The syntheses of these core materials are briefly described in the Supporting Information. First, the starting precursors L-cysteine (Loba Chemie, India), 3-(acryloyloxy)-2-hydroxypropyl methacrylate (AHPMA, Sigma-Aldrich, USA), dimethylphenylphosphine (DMPP, Sigma-Aldrich, USA), and ethyl acetate (Loba Chemie, India) were used for the preparation of cysteine methacrylate monomers in this work. Second, 3-methacryloxypropyltrimethoxysilane (MPS, Sigma-Aldrich, USA), *N*,*N*′-methylenebisacrylamide (MBA, Sigma-Aldrich, USA), 2,2′-azobisisobutyronitrile (AIBN, 12 wt % in acetone, Sigma-Aldrich, USA), ammonia solution (25−28%, Merck, Germany), absolute ethanol (Merck, Germany), and acetonitrile (Labscan, Thailand) were employed in the surface grafting processes. Finally, indigo carmine (IC, Sigma-Aldrich, USA), methylene blue (MB, Merck, Germany), rhodamine B (RhB, Loba Chemie, India), and methyl orange (MO, KemAus, Australia) were adopted as model organic dyes.

2.2. Preparation of $MgFe_2O_4$/PCysMA and $MgFe_2O_4$@SiO_2/PCysMA Nanocomposites. *2.2.1. Preparation of Cysteine Methacrylate (CysMA) Monomer.* The CysMA monomer was synthesized via a selective thio-Michael addition reaction as in previous work reported by Ladmiral et al.[23] In brief, 1.90 g of L-cysteine was dissolved in 15 mL of deionized water, and 3.25 mL of AHPMA was then added. Subsequently, 2.13 μL of DMPP was added to the mixture and stirred at 20 °C for 2 h. A colorless solution was obtained. To remove the unreacted organic species in the reaction mixture, ethyl acetate was added to the mixture three times to extract the organic species from the aqueous phase to an organic phase. The aqueous phase containing the product was then freeze-dried to obtain white powders. As shown in Figures S1 and S2 of the Supporting Information, ^{1}H NMR and ^{13}C NMR chemical shifts confirmed the successful preparation of the CysMA monomer, in agreement with previous studies.[23,32,33]

2.2.2. Synthesis of the $MgFe_2O_4$/PCysMA Nanocomposite. The $MgFe_2O_4$/PCysMA nanocomposite was prepared via two major steps: (i) surface functionalization of $MgFe_2O_4$ NPs by MPS to prepare MPS-immobilized $MgFe_2O_4$ ($MgFe_2O_4$−MPS) NPs and (ii) surface grafting of $MgFe_2O_4$−MPS NPs by

https://doi.org/10.1021/acs.iecr.2c03206
Ind. Eng. Chem. Res. 2022, 61, 18744−18761

Table 1. Chemical Structures and Maximum Absorption Wavelengths (λ_{max}) for the Selected Model Dyes

Dye classification	Dye	Chemical structure	λ_{max} (nm)
Cationic dyes	MB	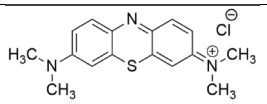	664
	RhB	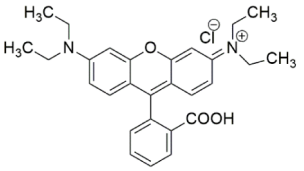	554
Anionic dyes	IC	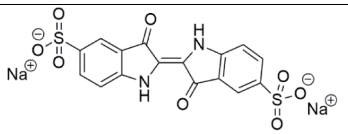	611
	MO	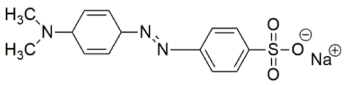	464

the radical polymerization of the CysMA monomer to obtain the $MgFe_2O_4$/PCysMA nanocomposite. The synthetic process is shown in Scheme 2. First, surface functionalization (i) of $MgFe_2O_4$ NPs was performed via hydrolysis and condensation of the vinyl silane coupling agent (i.e., MPS) using a method reported by Chen et al.[34] to form active C═C bonds on the surfaces. Briefly, 400 mg of $MgFe_2O_4$ powder was dispersed in a mixture of 50 mL of absolute ethanol, 12.5 mL of deionized water, and 1.50 mL of ammonia solution. After that, 0.80 mL of MPS was added to the mixture and stirred at 40 °C for 12 h. The product was separated from the mixture with an external magnet and then washed with deionized water and ethanol. The final product was dried in an open-air oven at 60 °C for 12 h.

Later, surface grafting (ii) of $MgFe_2O_4$−MPS NPs by PCysMA was performed using the method reported by Ji et al. with modification.[28] The $MgFe_2O_4$/PCysMA nanocomposite was prepared by one-step distillation-precipitation polymerization of the CysMA monomer in a mixture of acetonitrile and deionized water using MBA and AIBN as crosslinker and initiator, respectively. Two hundred milligrams of $MgFe_2O_4$−MPS powder were dispersed in 160 mL of acetonitrile/deionized water (6:4 v/v). Afterward, 960 mg of CysMA monomer, 200 mg of MBA, and 210 μL of AIBN solution were injected into the mixture. After mixing the solution for 20 min, the reaction mixture was heated to ∼80 °C and maintained for an hour under the distillation process. The product was separated from the mixture with an external magnet and washed with deionized water and ethanol three times. The final product was dried in an open-air oven at 60 °C for 12 h.

2.2.3. Synthesis of the $MgFe_2O_4$@SiO_2/PCysMA Nanocomposite. The $MgFe_2O_4$@SiO_2/PCysMA nanocomposite was synthesized by using the procedure described in Section 2.2.2, except $MgFe_2O_4$@SiO_2 powder was used instead of the $MgFe_2O_4$ powder.

2.3. Characterization. The chemical structure of the CysMA monomer was carefully identified by ^{1}H NMR and ^{13}C NMR (Bruker NEO 500 MHz) using deuterium oxide (D_2O) as the solvent. Phase formation of the as-synthesized nanocomposites was examined by performing X-ray diffraction (XRD, Rigaku SmartLab) using Cu Kα (λ = 1.5406 Å) irradiation with 0.02° scan steps over 2θ ranging from 10 to 90°. The morphologies of the nanocomposites were investigated by transmission electron microscopy (TEM, JEOL JEM-2010) using an accelerating voltage of 200 kV and field emission scanning electron microscopy (FE-SEM, JEOL JSM-IT800). The functional groups of the nanocomposites were explored by attenuated total reflectance−Fourier transform infrared spectroscopy (ATR−FTIR, Bruker TENSOR 27) run from 400 to 4000 cm^{-1}. The surface chemical compositions of the nanocomposites were analyzed by X-ray photoelectron spectroscopy (XPS, Kratos AXIS Ultra DLD) with a monochromatic Al Kα X-ray source (1486.6 eV). The C 1s peak at 285.0 eV was used as an internal reference standard. ζ potential measurements were performed at room temperature with a Zetasizer Nano ZS (Brookhaven, ZetaPALS) by adjusting the pH of the dispersion from 2 to 10 using 0.1 mol L^{-1} HCl and NaOH solutions. The ionic strengths of dispersions containing 0.1 mg mL^{-1} nanocomposites were adjusted to 1 × 10^{-3} mol L^{-1} using sodium chloride. The magnetic properties of the samples were revealed with a vibrating sample magnetometer (VSM, LakeShore VSM 7300 Series with LakeShore 735 Controller and LakeShore 450 Gaussmeter; Software Version 3.8.0) at room temperature using an applied field range of ±10 kOe. The specific surface areas and pore sizes of the nanocomposites were determined by N_2 adsorption−desorption with a surface area and pore size analyzer (Quantachrome model Autosorp 1 MP) using the Brunauer−Emmett−Teller (BET) and Barrett−Joyner−Halenda (BJH) methods, respectively. The samples were dehydrated at 110 °C before analysis. The effects of heating the as-synthesized nanocomposites were determined by thermogravimetric analysis (TGA, Rigaku, Thermo plus EV2). The samples were heated at temperatures ranging from 30 to 800 °C with a heating rate of 20 °C min^{-1} under a nitrogen atmosphere.

2.4. Adsorption of Dyes by $MgFe_2O_4$/PCysMA and $MgFe_2O_4$@SiO_2/PCysMA Nanocomposites. *2.4.1. Effect of Dye Solution Initial pH.* A comparative study of dye adsorption was performed with pristine adsorbents ($MgFe_2O_4$ and $MgFe_2O_4$@SiO_2 NPs) and modified adsorbents ($MgFe_2O_4$/PCysMA and $MgFe_2O_4$@SiO_2/PCysMA

https://doi.org/10.1021/acs.iecr.2c03206
Ind. Eng. Chem. Res. 2022, 61, 18744−18761

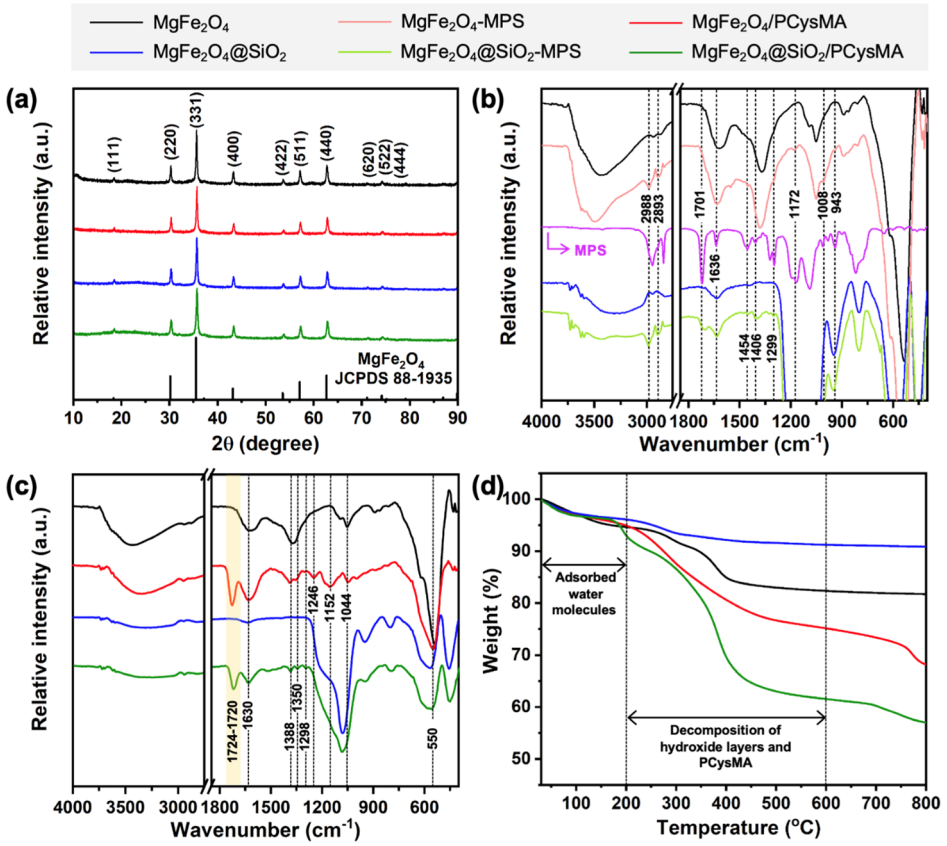

Figure 1. (a) XRD patterns, (b,c) FTIR spectra, and (d) TGA curves of $MgFe_2O_4$ NPs and $MgFe_2O_4$@SiO_2 NPs before and after polymerization of the CysMA monomer.

nanocomposites). The organic dyes, MB and IC, were used to model the behavior of cationic and anionic adsorbates, respectively. In this section, the effect of the initial dye solution pH on dye adsorption by the adsorbents was studied in batch adsorption experiments. Typically, 42 mg of adsorbent was mixed with 15 mL of 10 mg L^{-1} dye solution while varying the initial pH of the solution from ∼2 to ∼10 using 0.1 mol L^{-1} sodium hydroxide and nitric acid. Then, the mixture was shaken in a shaking water bath (DAIHAN Scientific, WSB-45) at 25 °C for 3 h. At the end of the adsorption process, the adsorbent was collected from the dye solution by using magnetic separation. UV−vis absorption spectra of the separated dye solution were recorded with a UV−vis spectrophotometer (PG Instrument, T80) to determine the absorbance values at the maximum absorption wavelengths of the model dyes (see Table 1). The removal efficiency and the amount of dye adsorbed on the adsorbent at the equilibrium state (q_e) were calculated using the following equations.

$$\text{removal efficiency}\ (\%) = [(C_0 - C_e)/C_0] \times 100 \quad (1)$$

$$q_e\ (\text{mg g}^{-1}) = [(C_0 - C_e)/m] \times V \quad (2)$$

where C_0 and C_e are the dye concentrations (mg L^{-1}) at the initial and equilibrium states, respectively, and m and V are the dry weight of the adsorbent (g) and volume of the dye solution (L), respectively.

2.4.2. pH-Selective Adsorption of Dyes. Selectivities of the adsorbents for the adsorption of dyes were examined using single and binary systems of dye adsorbates. The single-component systems were composed of 10 mg L^{-1} individual dyes (i.e., IC, MO, RhB, and MB). The initial pHs of the single dye solutions were adjusted to ∼2 and ∼10. The binary systems contained two dyes (i.e., IC/MO, IC/RhB, MB/MO, and MB/RhB). The mixtures of dyes containing 10 mg L^{-1} of each dye component were adjusted to initial pHs of ∼2 and ∼10 for the IC/MO and IC/RhB and MB/MO and MB/RhB solutions, respectively. To further confirm the pH-selective adsorption of dyes from the binary systems, IC/MO, IC/RhB, MB/MO, and MB/RhB solutions containing 500 mg L^{-1} of each dye component were also used as adsorbates. The procedure for adsorption experiments was described earlier in Section 2.4.1.

2.4.3. Adsorption Isotherms. Batch adsorption experiments were carried out in the manner described in Section 2.4.1, except the dye solutions contained various initial concentrations (i.e., 10−1000 mg L^{-1}). In addition, the initial pH values of the IC and MB solutions were kept constant at ∼2 and ∼10, respectively.

2.5. Reusability and Stability of $MgFe_2O_4$/PCysMA and $MgFe_2O_4$@SiO_2/PCysMA Nanocomposites. To investigate the reusability of the nanocomposites, careful adsorption−desorption studies were performed. In the first cycle of the adsorption process, 42 mg of the fresh nanocomposites (i.e., $MgFe_2O_4$/PCysMA and $MgFe_2O_4$@SiO_2/PCysMA) were mixed with 15 mL of 10 mg L^{-1} dye solution (i.e., IC at pH ∼2 and MB at pH ∼10). The mixture was shaken at 25 °C for 3 h. After that, the nanocomposites were separated from the dye solution by using magnetic separation. Absorption spectra of the dye solutions were collected using a UV−vis spectrophotometer to calculate the

https://doi.org/10.1021/acs.iecr.2c03206
Ind. Eng. Chem. Res. 2022, 61, 18744−18761

removal efficiencies of dyes. The dye-loaded nanocomposites were dried in an air oven at 60 °C overnight. The first cycle of the desorption process was then carried out by adding the dried nanocomposites into absolute ethanol at pH ∼2 and ∼10 (i.e., by adjusting by 0.1 mol L^{-1} sodium hydroxide and nitric acid) for desorption of MB and IC dyes, respectively. The mixture was then shaken at 25 °C for 3 h. After the desorption process, the nanocomposites were magnetically separated and then dried in an air oven at 60 °C for 6 h prior to further use in the next adsorption process. In this study, five adsorption−desorption cycles were monitored for each assay.

3. RESULTS AND DISCUSSION

3.1. Characterization of $MgFe_2O_4$/PCysMA and $MgFe_2O_4$@SiO_2/PCysMA Nanocomposites. XRD patterns of $MgFe_2O_4$ and $MgFe_2O_4$@SiO_2 NPs before and after polymerization of the CysMA monomer were collected to identify phase formation, as shown in Figure 1a. All diffraction patterns of the as-prepared materials were well matched with JCPDS card no. 88-1935 for $MgFe_2O_4$ without any impurities.[25] The results indicated that the pure cubic spinel phase of $MgFe_2O_4$ was still obtained after the polymerization process. In addition, the polymerization process did not affect the phase formation of $MgFe_2O_4$.

To determine the formation of the designed composites, the functionalization of $MgFe_2O_4$ and $MgFe_2O_4$@SiO_2 NPs by PCysMA was investigated with FTIR spectroscopy. Before grafting PCysMA onto the surfaces of $MgFe_2O_4$ and $MgFe_2O_4$@SiO_2 NPs, MPS was attached to their surfaces to form C═C bonds for further polymerization reactions. In Figure 1b, the FTIR spectra of the MPS-modified nanoparticles (i.e., $MgFe_2O_4$−MPS and $MgFe_2O_4$@SiO_2−MPS) showed the characteristic bands at ∼1636 and ∼1454 cm^{-1} assigned to C═C stretching and bending vibration modes of the immobilized MPS moieties.[35,36] Adsorbed water of MPS-unmodified nanoparticles showed the band at ∼1630 cm^{-1}, an overlapping band between the MPS, and adsorbed water was observed.[29,37,38] The surface modification of the magnetic nanoparticles by MPS can be further confirmed by the bands at ∼2988, ∼2893, and ∼1299 cm^{-1}, corresponding to stretching and bending vibration modes of C−H bonds of the MPS.[39] Apart from the FTIR result, the successful surface modification of $MgFe_2O_4$ and $MgFe_2O_4$@SiO_2 NPs by MPS was confirmed by a change of their surface properties, hydrophilicity to hydrophobicity (see Figure S3). Figure 1c shows FTIR spectra of $MgFe_2O_4$ and $MgFe_2O_4$@SiO_2 NPs before and after polymerization of the CysMA monomer. After grafting PCysMA onto the surfaces of $MgFe_2O_4$ and $MgFe_2O_4$@SiO_2 NPs, a new band at ∼1720 cm^{-1} was detected, and this was attributed to the C═O stretching mode of PCysMA.[40] In addition, bands at ∼1630, ∼1388, ∼1350, ∼1246, ∼1152, and ∼1044 cm^{-1} were assigned to N−H asymmetric bending, $-CH_2$ bending, O−C═O symmetric stretching, N−H bending, $-CH_2$ bending, and C−N stretching modes, respectively. These bands corresponded to cysteine embedded in the PCysMA matrix.[41] Some of those bands cannot be detected from the PCysMA-grafted $MgFe_2O_4$@SiO_2 NPs due to overlap with the strong characteristic bands of silica at ∼1270 to ∼980 cm^{-1} (i.e., stretching and bending modes of siloxane (Si−O−Si) and silanol (Si−OH) groups).[42] Furthermore, the band at ∼550 cm^{-1} was assigned to vibrational modes of metal oxides (i.e., Mg−O and Fe−O).[43] According to the FTIR results, $MgFe_2O_4$ and $MgFe_2O_4$@SiO_2 NPs were successfully composited with PCysMA.

Furthermore, the thermal properties of $MgFe_2O_4$ and $MgFe_2O_4$@SiO_2 NPs before and after grafting with PCysMA were also determined with TGA analysis, as illustrated in Figure 1d. In general, all samples showed two stages of weight loss at temperatures ranging from 30 to 600 °C under a nitrogen atmosphere. In the first stage, ∼3% weight loss occurred below 200 °C for all samples due to the loss of adsorbed water molecules from their surfaces.[44] In the second stage, ∼8 and ∼4% weight losses were obtained from 200 to 600 °C for $MgFe_2O_4$ NPs and $MgFe_2O_4$@SiO_2 NPs, respectively, and these were attributed to dehydroxylation of the hydroxide layers attached to the surfaces of the nanoparticles.[45,46] Furthermore, the weight losses increased to ∼18 and ∼28% for $MgFe_2O_4$/PCysMA and $MgFe_2O_4$@SiO_2/PCysMA nanocomposites, respectively, indicating degradation of the polymeric backbone of PCysMA.[44,46] Interestingly, the weight loss of the $MgFe_2O_4$@SiO_2/PCysMA nanocomposite was higher than that of the $MgFe_2O_4$/PCysMA nanocomposite. This could imply that the amount of PCysMA grafted on the $MgFe_2O_4$@SiO_2 NPs was higher than that on the $MgFe_2O_4$ NPs. This statement was also supported by the higher increase in mass for the $MgFe_2O_4$@SiO_2/PCysMA nanocomposite (i.e., ∼17% product recovery) compared to that for the $MgFe_2O_4$/PCysMA nanocomposite (i.e., ∼6% product recovery) after the PCysMA grafting process. TGA analyses also confirmed successful syntheses of $MgFe_2O_4$/PCysMA and $MgFe_2O_4$@SiO_2/PCysMA nanocomposites, in good agreement with the FTIR results.

The surface charge properties of the as-obtained nanocomposites were examined by ζ potential analysis, as shown in Figure 2a. The pHs at the point of zero charges (pH_{PZC}) for $MgFe_2O_4$/PCysMA and $MgFe_2O_4$@SiO_2/PCysMA nanocomposites were ∼5.0 and ∼5.6, respectively. The pH_{PZC} values of the as-synthesized nanocomposites were quite close to the isoelectric point of cysteine (5.07)[47] and similar to that of the PCysMA-grafted membrane (∼5.3) reported by Valencia et al.[40] In addition, the changes in pH_{PZC} values for the $MgFe_2O_4$/PCysMA and $MgFe_2O_4$@SiO_2/PCysMA nanocomposites were compared to those of pristine nanoparticles. The pH_{PZC} value of $MgFe_2O_4$/PCysMA nanocomposites was lower than that of $MgFe_2O_4$ NPs (∼8.4),[30] whereas the pH_{PZC} value of $MgFe_2O_4$@SiO_2/PCysMA nanocomposites was higher than that of $MgFe_2O_4$@SiO_2 NPs (∼4.9).[31] This indicated that after the polymerization process, the surface properties of the pristine nanoparticles were changed due to the grafting of PCysMA onto their surfaces.

Hysteresis loops illustrating the magnetic properties of $MgFe_2O_4$ and $MgFe_2O_4$@SiO_2 NPs before and after polymerization of the CysMA monomer were collected by VSM measurements at room temperature, as shown in Figure 2b. The saturation magnetization (M_s) values of $MgFe_2O_4$, $MgFe_2O_4$/PCysMA, $MgFe_2O_4$@SiO_2, and $MgFe_2O_4$@SiO_2/PCysMA powders were ∼39.5, ∼39.5, ∼35.5, and ∼25.5 emu g^{-1}, respectively. The M_s value of the $MgFe_2O_4$ NPs decreased from ∼39.5 to ∼35.5 emu g^{-1} after encapsulation with silica and then further decreased to ∼25.5 emu g^{-1} after polymerization of the CysMA monomer. The reduction in magnetization is attributed to the surface functionalization of magnetic nanoparticles by nonmagnetic materials (e.g., silica and polymers).[29,34] In contrast, no significant change in the M_s value for the $MgFe_2O_4$ NPs was observed after surface grafting

https://doi.org/10.1021/acs.iecr.2c03206
Ind. Eng. Chem. Res. 2022, 61, 18744−18761

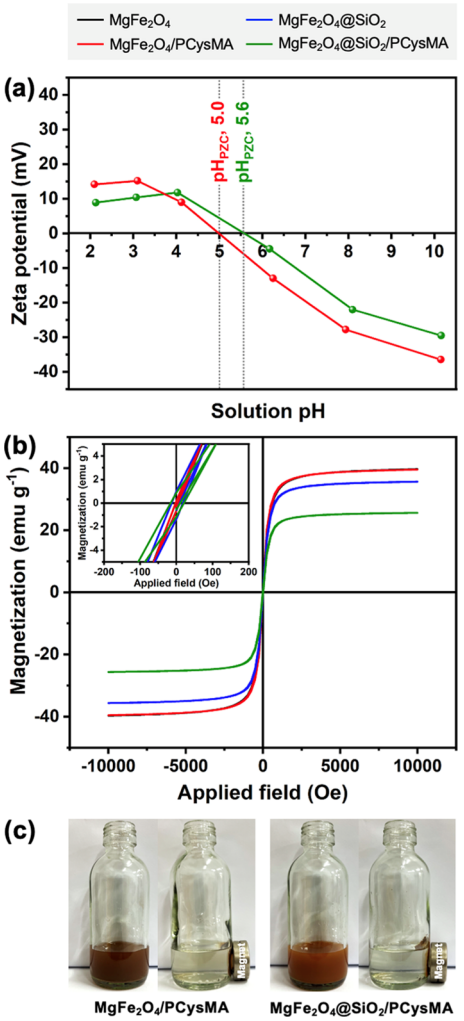

Figure 2. (a) ζ potential curves, (b) hysteresis loops, and (c) digital photographs demonstrating the magnetic separation of $MgFe_2O_4$ NPs and $MgFe_2O_4$@SiO_2 NPs before and after polymerization of the CysMA monomer.

with PCysMA. This could be due to a smaller amount of PCysMA grafted on $MgFe_2O_4$ surfaces compared to $MgFe_2O_4$@SiO_2, as described in the TGA results. However, all hysteresis loops exhibited a near zero remanence and coercivity (see inset of Figure 2b), indicating superparamagnetic behavior.[48,49] In addition, the $MgFe_2O_4$/PCysMA and $MgFe_2O_4$@SiO_2/PCysMA nanocomposites can be rapidly separated from the solution within a few minutes by using an external magnet, indicating an excellent magnetic response (see Figure 2c).

The morphologies of $MgFe_2O_4$ and $MgFe_2O_4$@SiO_2 NPs before and after polymerization of the CysMA monomer were explored by FE-SEM and TEM, as shown in Figure 3. In general, SEM images revealed spherical shapes with particle aggregation in all samples. The surfaces of $MgFe_2O_4$@SiO_2 NPs were smoother than those of $MgFe_2O_4$ NPs (see inset of Figure 3). In addition, the high-magnified TEM image of the $MgFe_2O_4$@SiO_2 NPs clearly showed an encapsulation of the $MgFe_2O_4$ core with a thin shell of silica. After grafting with PCysMA, TEM images showed that the $MgFe_2O_4$/PCysMA and $MgFe_2O_4$@SiO_2/PCysMA nanocomposites underwent more aggregation of particles than the pristine nanoparticles.

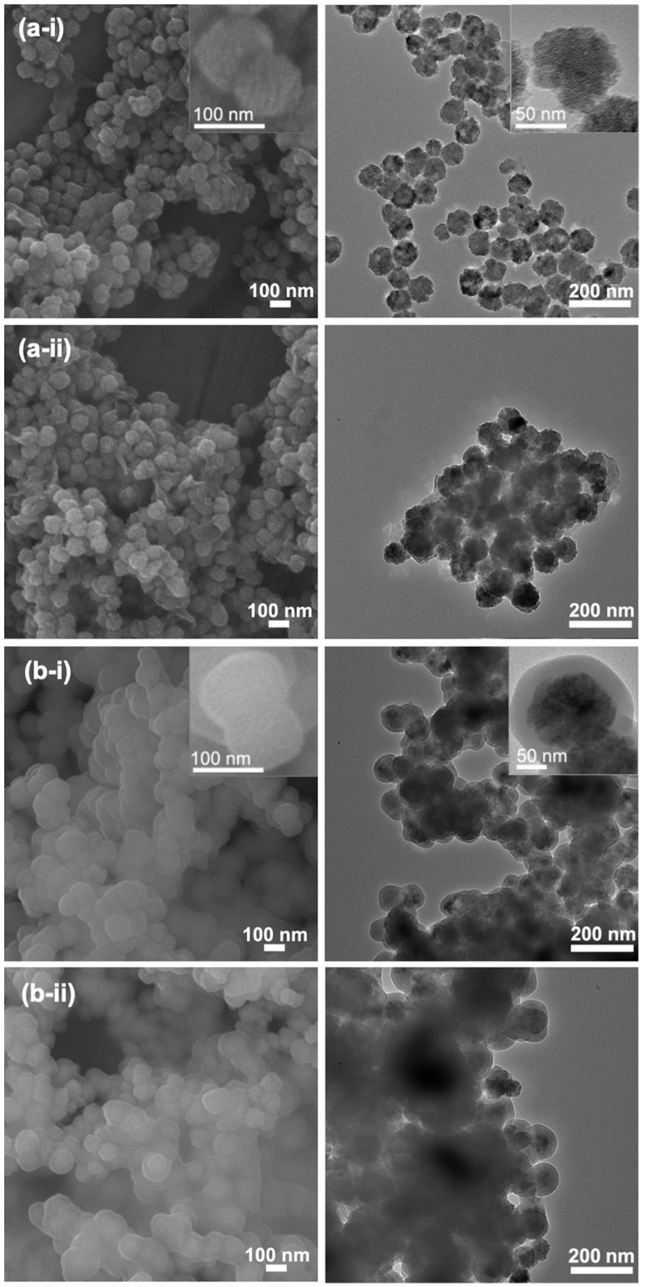

Figure 3. (left) FE-SEM and (right) TEM images of (a) $MgFe_2O_4$ and (b) $MgFe_2O_4$@SiO_2 NPs (i) before and (ii) after polymerization of the CysMA monomer.

This indicated that particle aggregation occurred after the polymerization process, as reported in the literature.[34,50]

The N_2 adsorption−desorption isotherms and pore size distributions of $MgFe_2O_4$ and $MgFe_2O_4$@SiO_2 NPs before and after grafting with PCysMA are presented in Figure 4. The pore size distributions of all samples ranged from ∼2 to ∼30 nm, demonstrating the mesoporous nature of the nanoadsorbents.[43] In addition, the BET-specific surface areas (S_{BET}), average pore sizes, and pore volumes of the as-synthesized samples are listed in Table 2. After polymerization of the CysMA monomer, the S_{BET} values of the as-obtained nanocomposites decreased compared to those of the pristine nanoparticles. This could be due to the blocking of some pores and aggregation of nanoparticles during the polymerization process.[50−53]

https://doi.org/10.1021/acs.iecr.2c03206
Ind. Eng. Chem. Res. 2022, 61, 18744−18761

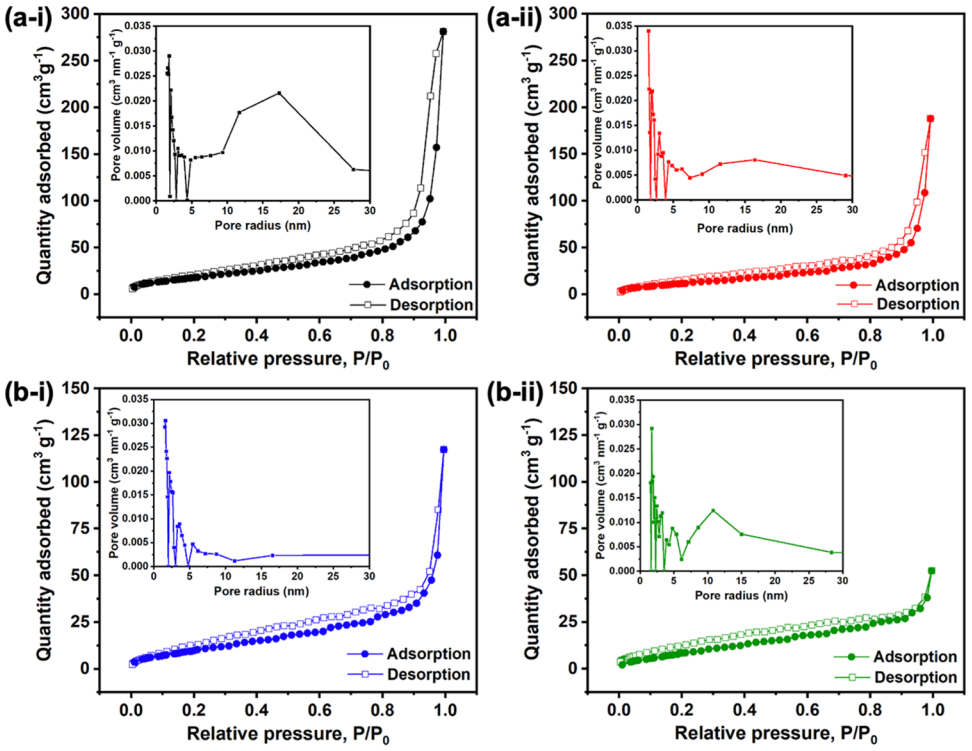

Figure 4. N_2 adsorption−desorption isotherms and pore size distribution with pore volume (inset) of (a) $MgFe_2O_4$ NPs and (b) $MgFe_2O_4$@SiO_2 NPs (i) before and (ii) after polymerization of the CysMA monomer.

Table 2. BET-Specific Surface Area (S_{BET}), Average Pore Radius, and Pore Volume of the as-Obtained Samples

sample	S_{BET} ($m^2\ g^{-1}$)	average pore radius (nm)	specific pore volume ($cm^3\ g^{-1}$)
$MgFe_2O_4$	72.1	12.1	0.44
$MgFe_2O_4$@SiO_2	43.3	8.4	0.18
$MgFe_2O_4$/PCysMA	53.8	10.8	0.29
$MgFe_2O_4$@SiO_2/PCysMA	40.1	4.0	0.08

The surface compositions of the as-prepared samples were examined by XPS. Survey and high-resolution XPS spectra are provided in Figure 5. All survey spectra (see Figure 5a,d) exhibited the presence of Mg, Fe, and O elements, which was consistent with the chemical compositions of the $MgFe_2O_4$ NPs. However, Si was detected in $MgFe_2O_4$@SiO_2 NPs due to surface coating by silica. The signals for N and S elements were detected in the spectra of $MgFe_2O_4$/PCysMA and $MgFe_2O_4$@SiO_2/PCysMA nanocomposites and were attributed to PCysMA grafted on their surfaces.[30,40] However, the signal for N was also found for the $MgFe_2O_4$ NPs due to the ethanolamine used to prepare them. In the high-resolution N 1s XPS spectrum of $MgFe_2O_4$ NPs (see Figure 5b), the signal at ∼399.7 eV was assigned to $-NH_2$ groups from the ethanolamine molecules.[30] Two chemical species were detected in the N 1s spectra for both $MgFe_2O_4$/PCysMA and $MgFe_2O_4$@SiO_2/PCysMA nanocomposites (see Figure 5b,e). The bands at ∼399.5 and ∼401.2 eV corresponded to free amine ($-NH_2$) and aminium ($-NH_3^+$), respectively.[32,40] In addition, S was detected in these nanocomposites due to the sulfur bridges of the PCysMA matrix.[32] The S 2p signals at ∼163.2 and ∼164.3 eV (see Figure 5c,f) were assigned to S $2p_{3/2}$ and S $2p_{1/2}$ ionizations, respectively.[32] Therefore, the XPS results indicated successful grafting of PCysMA onto the $MgFe_2O_4$ and $MgFe_2O_4$@SiO_2 NPs, which is consistent with the FTIR results. According to the combination of several characterization techniques (i.e., XRD, FTIR, TGA, ζ potential analysis, VSM, FE-SEM, TEM, N_2 adsorption−desorption isotherm, and XPS), the $MgFe_2O_4$/PCysMA and $MgFe_2O_4$@SiO_2/PCysMA nanocomposites were successfully prepared. The as-prepared nanocomposites were further used as adsorbents to study the adsorption of dyes from single-component and binary solutions, and the effects of the initial dye solution pH on pH-selective adsorption of dyes and their adsorption isotherms were determined.

3.2. Adsorption of Dyes by $MgFe_2O_4$/PCysMA and $MgFe_2O_4$@SiO_2/PCysMA Nanocomposites. *3.2.1. Effect of the Dye Solution Initial pH.* In general, the initial pH of the solution is one of the most important factors influencing the adsorption of a dye.[54] The solution pH affects the surface charges of adsorbents, which depend on the pH at the point of zero charges (pH_{PZC}). The adsorbent surfaces show net positive charges when the solution pH is less than pH_{PZC}. When the solution pH is above the pH_{PZC}, the adsorbent surfaces show net negative charges.[55] In this section, the effects of initial dye solution pH over the range ∼2 to ∼10 on the efficiencies for the removal of dyes by $MgFe_2O_4$ and $MgFe_2O_4$@SiO_2 NPs were investigated before and after surface modification by PCysMA with the use of anionic IC and cationic MB dyes as adsorbates. As illustrated in Figure 6a, the efficiencies for removal of IC (>90%) and MB (<10%) by the $MgFe_2O_4$ NPs were obtained over all pH ranges. These findings indicated that the adsorption of IC and MB by the unmodified $MgFe_2O_4$ NPs was independent of pH. In addition, the $MgFe_2O_4$ nanoadsorbent preferentially adsorbed the anionic IC dye rather than the cationic MB dye, as observed in a previous study.[56] The efficiency for removal of IC by the $MgFe_2O_4$/PCysMA nanoadsorbent decreased from

https://doi.org/10.1021/acs.iecr.2c03206
Ind. Eng. Chem. Res. 2022, 61, 18744−18761

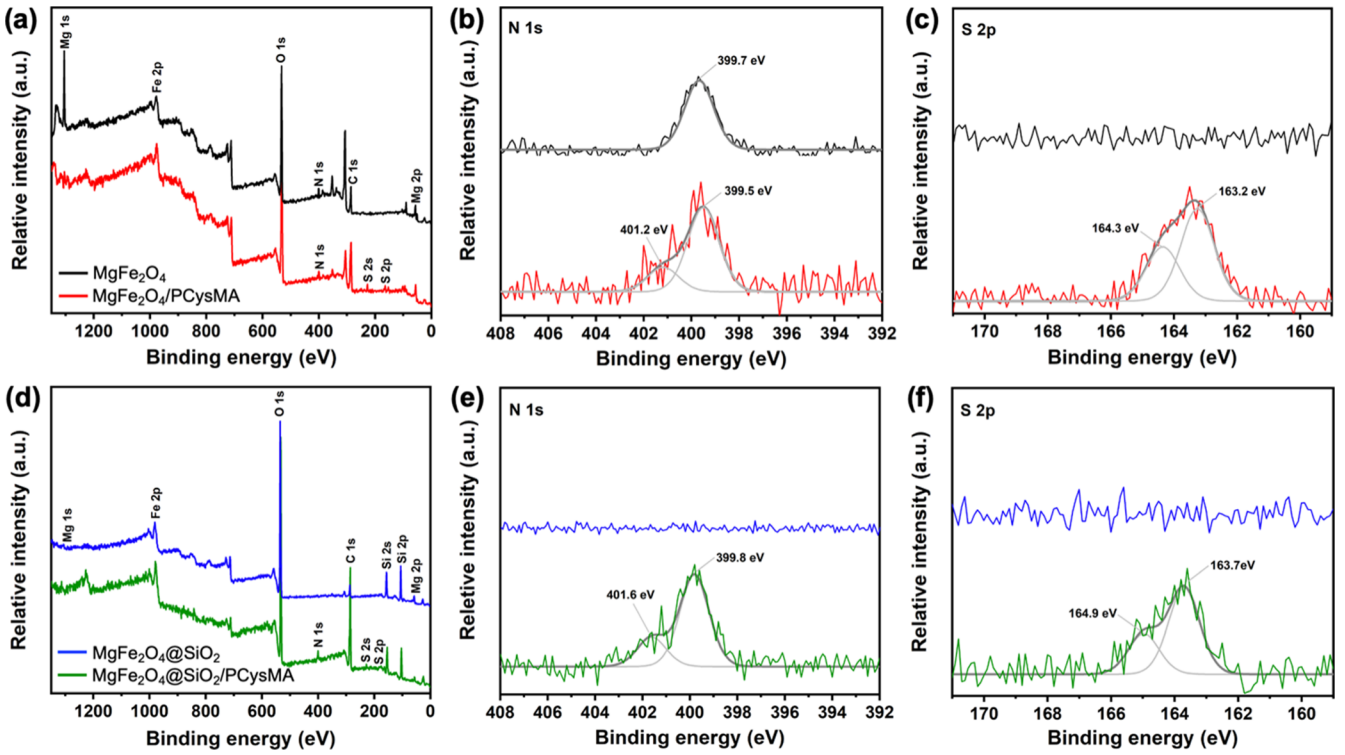

Figure 5. (a,d) Survey scan XPS spectra and high resolution (b,e) N 1s and (c,f) S 2p XPS spectra of $MgFe_2O_4$ NPs and $MgFe_2O_4$@SiO_2 NPs before and after polymerization of the CysMA monomer.

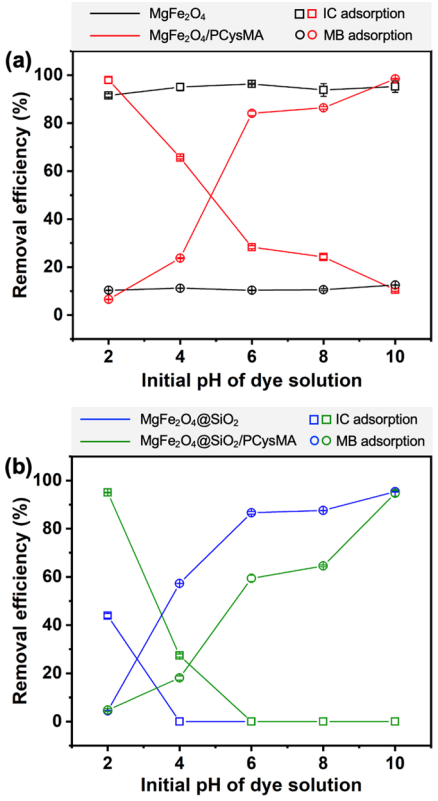

Figure 6. Effect of the initial dye solution pH on the efficiencies for the removal of IC and MB by pristine and modified (a) $MgFe_2O_4$ NPs and (b) $MgFe_2O_4$@SiO_2 NPs.

~95 to ~10% upon increasing the solution pH from ~2 to ~10. In contrast, the efficiency for removal of MB increased from ~7 to ~98% upon increasing the solution pH. The maximum efficiencies for removal of IC and MB by the $MgFe_2O_4$/PCysMA nanocomposite were obtained at pH ~2 and ~10, respectively. According to the pH_{PZC} of the $MgFe_2O_4$/PCysMA nanoadsorbent (~5.0), the surface of the nanoadsorbent presents a net positive charge at pH 2−4 ($pH < pH_{PZC}$), resulting in the electrostatic attraction of the anionic IC. However, at these pH values, low removal efficiencies for MB were observed due to electrostatic repulsion between the positively charged surface of the adsorbent and the positive charge of the MB molecule. With increases in the solution pH from ~6 to ~10, the charge of the adsorbent surface became more negative ($pH > pH_{PZC}$), leading to electrostatic attraction of the cationic MB and electrostatic repulsion of the anionic IC. The results suggested that adsorption of IC and MB by the $MgFe_2O_4$/PCysMA nanoadsorbent is pH-dependent and driven by electrostatic interactions, indicating that surface modification of the $MgFe_2O_4$ NPs by the polymer (i.e., PCysMA) can increase the removal efficiency for MB. Interestingly, the PCysMA-modified $MgFe_2O_4$ NPs selectively removed either anionic IC or cationic MB dye after tailoring the solution pH appropriately. Consequently, a pH-selective adsorbent was obtained.

The efficiencies for removal of IC and MB by the $MgFe_2O_4$@SiO_2 and $MgFe_2O_4$@SiO_2/PCysMA nanoadsorbents were also studied to investigate pH-dependent adsorption by the PCysMA-grafted nanoadsorbent, and the results are presented in Figure 6b. At pH ~2, the $MgFe_2O_4$@SiO_2 nanoadsorbent provided ~44% IC removal efficiency, whereas no adsorption of IC occurred upon increasing the solution pH from ~4 to ~10. For MB adsorption, the efficiencies for removal of MB by the $MgFe_2O_4$@SiO_2 nanoadsorbent increased significantly from ~4 to ~95% upon increasing the solution pH from ~2 to ~10. The maximum efficiencies for

https://doi.org/10.1021/acs.iecr.2c03206
Ind. Eng. Chem. Res. 2022, 61, 18744−18761

removal of IC (~44%) and MB (~95%) by the unmodified $MgFe_2O_4$@SiO_2 nanoadsorbent were obtained at pH ~2 and pH ~10, respectively. Based on the pH_{PZC} of the $MgFe_2O_4$@SiO_2 nanoadsorbent (~4.9),[31] the surface of the nanoadsorbent showed a net positive charge at pH ~2 (pH < pH_{PZC}), which resulted in the electrostatic attraction of the anionic IC. However, this nanoadsorbent exhibited moderate efficiency for the removal of IC, indicating low selectivity for the adsorption of IC. The low efficiency for the adsorption of MB by the $MgFe_2O_4$@SiO_2 NPs at pH ~2 was attributed to electrostatic repulsion between the positive charge of the adsorbent surface and the cationic MB. When the solution pH was increased, the surface charge of the adsorbent became more negative, leading to strong electrostatic attraction with the cationic MB. These findings suggested that the adsorption of IC and MB by the unmodified $MgFe_2O_4$@SiO_2 nanoadsorbent was pH dependent. Furthermore, this nanoadsorbent selectively adsorbed either IC or MB dyes by changing the solution pH appropriately. The efficiency for removal of IC by the $MgFe_2O_4$@SiO_2/PCysMA nanocomposites decreased significantly from ~95% to ~27% upon tuning the pH from ~2 to ~4. When the solution pH was increased from ~6 to ~10, no adsorption of IC was observed. For MB adsorption, the efficiency for removal by the $MgFe_2O_4$@SiO_2/PCysMA nanoadsorbent increased from ~4 to ~95% upon increasing the solution pH from ~2 to ~10. These observations indicated that the behavior of the $MgFe_2O_4$@SiO_2/PCysMA nanoadsorbent was pH dependent. The interactions between adsorbates, IC and MB, and the $MgFe_2O_4$@SiO_2/PCysMA nanoadsorbent can be explained by electrostatic interactions similar to those operating among the adsorbates, IC and MB, and the $MgFe_2O_4$/PCysMA nanoadsorbent. In addition, the $MgFe_2O_4$@SiO_2/PCysMA nanoadsorbent selectively adsorbed either IC or MB upon tuning the solution pH, similar to the unmodified $MgFe_2O_4$@SiO_2 nanoadsorbent. However, the PCysMA-modified $MgFe_2O_4$@SiO_2 NPs provided higher efficiency for the removal of IC than the unmodified $MgFe_2O_4$@SiO_2 NPs, suggesting more selectivity adsorption of IC.

In these studies, the PCysMA-modified nanoadsorbents (i.e., $MgFe_2O_4$/PCysMA and $MgFe_2O_4$@SiO_2/PCysMA) exhibited maximum efficiencies for the adsorption of IC and MB with initial solution pH values of ~2 and ~10, respectively. Interestingly, these composite nanoadsorbents showed pH-dependent selective adsorption and are considered promising materials for magnetic solid-phase extraction (MSPE) techniques used to detect/identify and quantify organic dyes in several samples (e.g., food and water).[9,57] In addition, selectivity for the extraction of the targeted molecules from samples is one of the most attractive characteristics with which to choose the adsorbent for the MSPE method.[58] Therefore, to determine the selectivities of $MgFe_2O_4$/PCysMA and $MgFe_2O_4$@SiO_2/PCysMA nanoadsorbents, adsorption of other dyes from single-component and binary dye systems was examined further as described in Section 3.2.2.

3.2.2. pH-Selective Adsorption of Dyes. To demonstrate pH-selective adsorption of dyes by $MgFe_2O_4$ and $MgFe_2O_4$@SiO_2 NPs before and after surface modification with PCysMA, adsorption of anionic (i.e., IC and MO) and cationic (i.e., MB and RhB) dyes from single-component dye systems were studied. The relative efficiencies for the removal of these dyes from single solutions at pH ~2 and ~10 are shown in Figure 7. The colors of the solutions for each dye before and after adsorption are also provided in Figure S4.

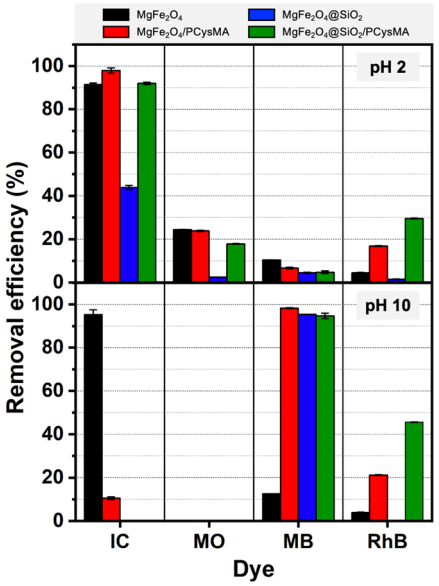

Figure 7. Relative efficiencies for the removal of IC, MO, MB, and RhB from single solutions with initial pH ~2 and pH ~10 by pristine and modified $MgFe_2O_4$ NPs and $MgFe_2O_4$@SiO_2 NPs.

A set of anionic dyes with high efficiencies (>90%) for removal of IC by the unmodified $MgFe_2O_4$ nanoadsorbent at pH ~2 and ~10 were obtained, indicating that this nanoadsorbent exhibited selective adsorption of IC without pH dependence. The efficiencies for removal of IC by unmodified $MgFe_2O_4$@SiO_2 NPs were ~44 and 0% at pH ~2 and ~10, respectively. This suggested that the $MgFe_2O_4$@SiO_2 nanoadsorbent exhibited weakly pH-selective adsorption of IC since only moderate removal efficiency was obtained with IC at pH ~2. After surface modification of the $MgFe_2O_4$ and $MgFe_2O_4$@SiO_2 NPs by PCysMA, the efficiencies for removal of IC by the PCysMA-modified nanoadsorbents significantly increased, to above 90% at pH ~2, compared to those of the unmodified NPs. At pH ~10, very low efficiencies for removal of IC by $MgFe_2O_4$/PCysMA (~10%) and $MgFe_2O_4$@SiO_2/PCysMA (0%) nanoadsorbents were obtained. Interestingly, these results indicated that the PCysMA-modified nanoadsorbents underwent pH-selective adsorption of IC. In addition, the $MgFe_2O_4$@SiO_2/PCysMA nanoadsorbent showed stronger pH-selective adsorption of IC than the $MgFe_2O_4$/PCysMA nanoadsorbent.

For MO adsorption, low efficiencies for removal of MO by unmodified $MgFe_2O_4$ (~24%) and $MgFe_2O_4$@SiO_2 (~2%) nanoadsorbents were observed at pH ~2. After grafting the $MgFe_2O_4$ surfaces with PCysMA, the efficiency for removal of MO was still low (~24%). However, increases in MO removal efficiencies from ~2 to ~18% were observed after surface modification of the $MgFe_2O_4$@SiO_2 NPs by the polymer. This showed that surface grafting by PCysMA improved the use of $MgFe_2O_4$@SiO_2 NPs as a MO adsorbent. MO adsorption by the PCysMA-modified $MgFe_2O_4$@SiO_2 NPs was attributed to the presence of PCysMA immobilized on the NP surfaces. In addition, the amount of the polymer on the $MgFe_2O_4$@SiO_2 surfaces was higher than that on the $MgFe_2O_4$ surfaces, as revealed by the TGA analyses.

https://doi.org/10.1021/acs.iecr.2c03206
Ind. Eng. Chem. Res. 2022, 61, 18744−18761

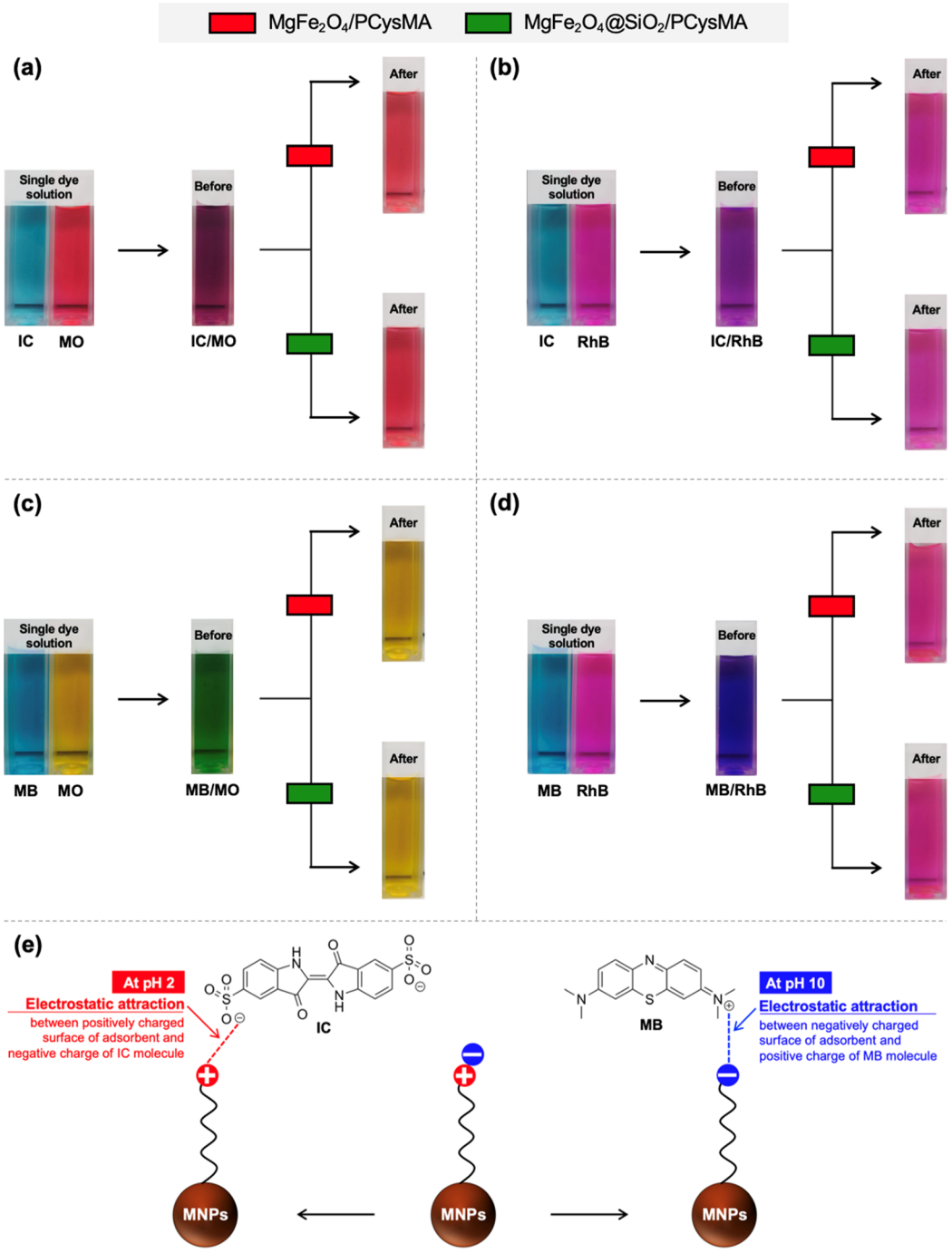

Figure 8. Colors of (a) IC/MO, (b) IC/RhB, (c) MB/MO, and (d) MB/RhB binary solutions before and after adsorption by the PCysMA-modified nanoadsorbents. (e) Proposed mechanism for the adsorption of IC and MB by the PCysMA-modified nanoadsorbents at pH 2 and 10.

Among a set of cationic dyes, low efficiencies (~10%) for removal of MB by the unmodified $MgFe_2O_4$ nanoadsorbent were obtained at both pH ~2 and ~10, resulting in non-pH-selective adsorption of MB. In contrast, the efficiencies for removal of MB by the unmodified $MgFe_2O_4$@SiO_2 nanoadsorbent were ~4 and ~95% at pH ~2 and ~10, respectively, indicating pH-selective adsorption of MB. After surface modification by PCysMA, high efficiencies for the adsorption of MB (>90%) were obtained at pH ~10 when using the $MgFe_2O_4$/PCysMA nanoadsorbent, indicating enhanced pH-selective adsorption of MB. However, no significant difference in the efficiencies for removal of MB by pristine and modified $MgFe_2O_4$@SiO_2 NPs was found at pH ~10, which was attributed to the low initial concentration of the MB solution. To prove this, the initial concentration of the MB solution was adjusted to ~300 mg L^{-1} at pH ~10. A high efficiency for removal of MB (~95%) by the $MgFe_2O_4$@SiO_2/PCysMA nanoadsorbent was observed, while only ~10% MB removal efficiency was seen for $MgFe_2O_4$@SiO_2 NPs (see Figure S5). It is seen that grafting $MgFe_2O_4$@SiO_2 NPs with PCysMA increased the removal efficiency for MB.

For RhB adsorption, low efficiencies (<5%) for removal of RhB by the unmodified $MgFe_2O_4$ nanoadsorbent were obtained at pH ~2 and ~10. Likewise, the unmodified

https://doi.org/10.1021/acs.iecr.2c03206
Ind. Eng. Chem. Res. 2022, 61, 18744−18761

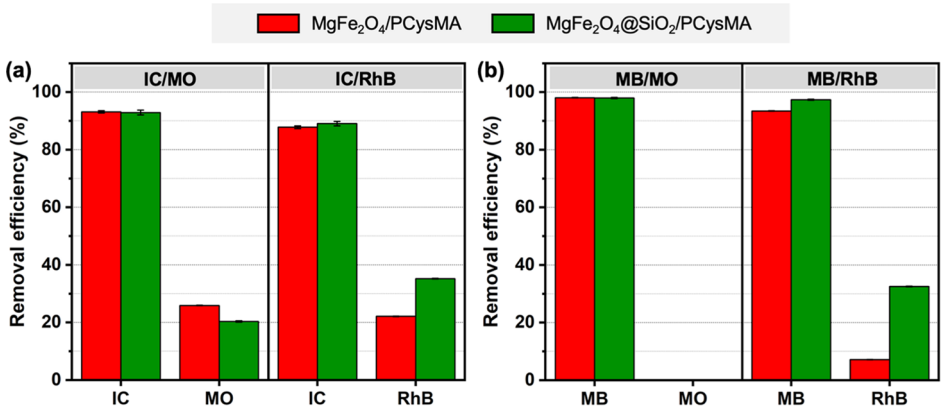

Figure 9. Relative efficiencies for the removal of dyes from binary systems by PCysMA-modified nanoadsorbents: (a) IC/MO and IC/RhB at pH ∼2 and (b) MB/MO and MB/RhB at pH ∼10.

$MgFe_2O_4$@SiO_2 nanoadsorbent exhibited no adsorption of RhB at these pH values. Interestingly, increases in the RhB removal efficiencies were observed after surface modifications of $MgFe_2O_4$ and $MgFe_2O_4$@SiO_2 NPs by PCysMA. Additionally, increases in the efficiencies for RhB removal by the $MgFe_2O_4$@SiO_2/PCysMA nanoadsorbent were higher than those of the $MgFe_2O_4$/PCysMA nanoadsorbent, owing to the higher amount of PCysMA contained on the $MgFe_2O_4$@SiO_2 surfaces. However, low-to-moderate efficiencies for the removal of RhB by the PCysMA-modified nanoadsorbents were obtained at pH ∼2 and ∼10, suggesting weakly pH-selective adsorption of RhB. In addition, neutral red (NR) was used as a representative neutral dye to further confirm the selectivity of the nanoadsorbents. As shown in Figure S6, low removal efficiencies of NR by $MgFe_2O_4$ NPs, $MgFe_2O_4$@SiO_2 NPs, and their nanocomposites were obtained at pH ∼2 and pH ∼10. The result indicated that all nanoadsorbents are ineffective for pH-selective adsorption of the neutral dye.

The mechanisms for the adsorption of anionic IC and MO dyes by the PCysMA-modified nanoadsorbents can be explained by the following interactions: (1) at pH ∼2, electrostatic attractions between the negatively charged sulfonate ($-SO_3^-$) groups on the dye molecules and positively charged protonated amine ($-NH_3^+$) groups on the surfaces of the nanoadsorbents and (2) at pH ∼10, electrostatic repulsions between the negatively charged $-SO_3^-$ groups on the dye molecules and negatively charged carboxyl ($-COO^-$) groups on the surfaces of the nanoadsorbents.[59,60] Moreover, the efficiencies for removal of IC by the PCysMA-modified nanoadsorbents at pH ∼2 were much higher than those for MO. Considering the chemical structures of the dyes (see Table 1), the IC molecule contains two $-SO_3^-$ groups, whereas MO has only one, which results in preferential adsorption of IC. In addition, IC contains secondary amine groups, which facilitate other interactions with the nanoadsorbent surfaces (i.e., hydrogen-bonding interactions).[61,62] In contrast, since the MO molecule contains a tertiary amine group, it is present as the protonated form at pH ∼2 (pK_a = 3.46), which hinders adsorption.[63] For the adsorption of cationic dyes (i.e., MB and RhB), the opposite mechanism can be proposed. In addition, the PCysMA-modified nanoadsorbents preferentially adsorbed MB rather than RhB at pH ∼10. Since the RhB molecule contains a carboxylic group, this group is deprotonated at pH > 3.7 (pK_a = 3.7), leading to electrostatic repulsions between the negative charge of the RhB molecule and the surfaces of the nanoadsorbents.[64]

In conclusion, in the studies of pH-selective adsorption for single dye systems at pH ∼2 and ∼10, the PCysMA-modified nanoadsorbents preferentially adsorbed anionic IC rather than anionic MO at pH ∼2, whereas these nanoadsorbents preferentially removed cationic MB rather than cationic RhB at pH ∼10. The results demonstrate that the PCysMA-modified nanoadsorbents exhibited pH-selective adsorption of anionic IC and cationic MB at pH ∼2 and ∼10, respectively.

To confirm pH-selective adsorption of IC (at pH ∼2) and MB (at pH ∼10) by the $MgFe_2O_4$/PCysMA and $MgFe_2O_4$@SiO_2/PCysMA nanocomposites, two sets of IC-based (i.e., IC/MB, IC/MO, and IC/RhB) and MB-based (i.e., MB/IC, MB/MO, and MB/RhB) binary solutions with 10 mg L^{-1} concentrations for each dye were used as adsorbates with pH values of ∼2 and ∼10, respectively. Unfortunately, a preliminary study showed that the absorption bands of IC and MB in the IC/MB mixture significantly changed in comparison with the absorption bands of these dyes in single-component dye systems (see Figure S7). This was probably due to chemical interactions between IC and MB since a precipitate was formed in the IC/MB mixture (data not provided). Therefore, all mixtures of dyes were tested in this study except for the IC/MB series. The colors of these binary solutions before and after adsorption by the nanocomposites are shown in Figure 8. The relative efficiencies for the removal of each dye from the binary solutions are also provided in Figure 9.

In the first set, the colors of the IC/MO and IC/RhB solutions changed to amaranth red and fuchsia, which were similar to the colors of the single MO and RhB dyes after the adsorption process (see Figure 8a,b). Correspondingly, high efficiencies for removal of IC (∼90%) by the $MgFe_2O_4$/PCysMA and $MgFe_2O_4$@SiO_2/PCysMA nanoadsorbents from both IC/MO and IC/RhB solutions were obtained, whereas these nanoadsorbents exhibited low efficiencies for removal of MO (<25%) and RhB (<35%), as illustrated in Figure 9a. These results indicated that the $MgFe_2O_4$/PCysMA and $MgFe_2O_4$@SiO_2/PCysMA nanoadsorbents preferentially adsorbed IC rather than MO or RhB from binary solutions of IC/MO and IC/RhB at pH ∼2, indicating highly pH-selective adsorption of IC. This result was in good agreement with the adsorption behaviors of dyes in the single-component dye systems. The higher efficiencies for removal of IC over MO

https://doi.org/10.1021/acs.iecr.2c03206
Ind. Eng. Chem. Res. 2022, 61, 18744−18761

Table 3. Langmuir and Freundlich Parameters for IC and MB Adsorption Onto Different Adsorbents

	IC					
	Langmuir isotherm			Freundlich isotherm		
adsorbent	q_m(mg/g)	K_L(L/mg)	R^2	K_F(mg (L mg^{-1})$^{1/n}$ g^{-1})	n	R^2
$MgFe_2O_4$	72.6	0.12	0.999	10.7	2.9	0.909
$MgFe_2O_4$/PCysMA	94.6	0.14	0.999	10.2	2.5	0.912
$MgFe_2O_4$@SiO_2	4.9	0.08	0.990	1.8	5.8	0.760
$MgFe_2O_4$@SiO_2/PCysMA	139.5	0.06	0.999	9.3	1.9	0.907
	MB					
	Langmuir isotherm			Freundlich isotherm		
adsorbent	q_m(mg/g)	K_L(L/mg)	R^2	K_F(mg (L mg^{-1})$^{1/n}$ g^{-1})	n	R^2
$MgFe_2O_4$	1.71	0.04	0.812	0.2	3.0	0.587
$MgFe_2O_4$/PCysMA	50.0	0.26	0.997	7.0	3.1	0.971
$MgFe_2O_4$@SiO_2	10.5	2.04	0.999	4.7	5.3	0.931
$MgFe_2O_4$@SiO_2/PCysMA	138.3	0.07	0.999	16.5	2.6	0.876

and RhB at pH ∼2 could be attributed to strong electrostatic attractions and hydrogen-bonding interactions, as mentioned for the single-component dye systems.[59,61,62] However, no significant differences were observed in the efficiencies for removal of IC from either IC/MO or IC/RhB solutions by the $MgFe_2O_4$/PCysMA and $MgFe_2O_4$@SiO_2/PCysMA nanoadsorbents, probably due to the low initial concentrations of these binary solutions.

To clearly indicate the high selectivity of the PCysMA-modified nanoadsorbents for IC adsorption from binary solutions, high initial concentrations of the IC/MO and IC/RhB solutions were used at pH ∼2. Since the maximum capacities for the adsorption of both IC and MB by the PCysMA-modified nanoadsorbents were obtained when using 500 mg L^{-1} initial concentrations for the dye solutions (data not provided), the initial concentrations for each dye in the binary solutions (i.e., IC/MO and IC/RhB) were set at 500 mg L^{-1}. With increases in the IC/MO concentrations to 500:500 mg L^{-1}, the efficiencies for removal of IC by the $MgFe_2O_4$/PcysMA and $MgFe_2O_4$@SiO_2/PCysMA nanoadsorbents decreased to ∼46 and ∼68%, respectively (see Figure S8a). Similarly, the $MgFe_2O_4$/PCysMA and $MgFe_2O_4$@SiO_2/PCysMA nanoadsorbents exhibited IC removal efficiencies of ∼51 and ∼72%, respectively, for IC/RhB solutions. Interestingly, no adsorption of MO or RhB occurred from either IC/MO or IC/RhB solutions. The results clearly demonstrated that the PCysMA-modified nanoadsorbents exhibited highly pH-selective adsorption of IC. In addition, the $MgFe_2O_4$@SiO_2/PCysMA nanoadsorbent showed an efficiency for the adsorption of IC higher than that of the $MgFe_2O_4$/PCysMA nanoadsorbent, suggesting higher selectivity for the adsorption of IC.

In the second set, the colors of the MB/MO and MB/RhB solutions turned yellow and fuchsia, similar to the colors of the single MB and RhB dyes after adsorption (see Figure 8c,d). As shown in Figure 9b, high efficiencies (>90%) were observed for the removal of MB from both MB/MO and MB/RhB solutions by the $MgFe_2O_4$/PCysMA and $MgFe_2O_4$@SiO_2/PCysMA nanoadsorbents, which was consistent with the changes in the colors of these solutions. In addition, the PCysMA-modified nanoadsorbents exhibited no adsorption of MO from the MB/MO solution, indicating highly pH-selective adsorption of MB from the MB/MO solution. However, low efficiencies for the removal of RhB by the $MgFe_2O_4$/PCysMA (∼7%) and $MgFe_2O_4$@SiO_2/PCysMA (∼33%) nanoadsorbents were still obtained for the MB/RhB solutions (see Figure 9b). This result indicated that the PCysMA-modified nanoadsorbents preferentially adsorbed MB rather than RhB from the MB/RhB solutions at pH ∼10, similar to the results obtained for the single-component dye systems. Higher efficiencies for removal of MB over MO and RhB at pH ∼10 could be caused by strong electrostatic attractions, as previously described for the single-component dye system.[60,65]

To clearly demonstrate the selectivities of the nanoadsorbents for the adsorption of MB from the binary solutions, a further study of MB adsorption from MB-based binary solutions was undertaken with 500 mg L^{-1} initial concentrations for each dye and the PCysMA-modified nanoadsorbents at pH ∼10. As illustrated in Figure S8b, the efficiencies for removal of MB from 500:500 mg L^{-1} MB/RhB solutions by $MgFe_2O_4$/PCysMA and $MgFe_2O_4$@SiO_2/PCysMA decreased to ∼29 and ∼76%, respectively. In addition, there was no adsorption of RhB from the MB/RhB solutions. These results clearly indicated that the PCysMA-modified nanoadsorbents exhibited high selectivity for the adsorption of MB from an MB/RhB solution at pH ∼10. Interestingly, at 500:500 mg L^{-1} concentrations for both MB/MO and MB/RhB solutions, the $MgFe_2O_4$@SiO_2/PCysMA nanoadsorbent provided higher efficiencies for the removal of MB than the $MgFe_2O_4$/PCysMA nanoadsorbent, indicating more selective adsorption of MB. This finding was consistent with the adsorption of IC from the IC-based binary solutions. The highly pH-selective adsorptions of IC and MB by the $MgFe_2O_4$@SiO_2/PCysMA nanoadsorbent could be due to the higher amount of PCysMA present on the surfaces of $MgFe_2O_4$@SiO_2 NPs compared to the $MgFe_2O_4$ NPs.

The key findings obtained in this section are as follows. The PCysMA-grafted nanoadsorbents exhibited highly pH-selective adsorption of IC (at pH ∼2) and MB (at pH ∼10) from both single and binary dye solutions. The highly pH-selective adsorption of IC and MB could be rationalized by the presence of $-NH_3^+$ and $-COO^-$ groups on the surfaces of the nanoadsorbents, which led to the strong electrostatic attraction for the IC and MB molecules, as provided in Figure 8e. In addition, the grafting of PCysMA on the $MgFe_2O_4$@SiO_2 NPs resulted in higher pH-selective adsorption of these dyes compared to $MgFe_2O_4$ NPs. The highly selective pH-dependent adsorptions of IC and MB can be rationalized by the presence of PCysMA and the large amounts of grafted PCysMA in the nanocomposites.

https://doi.org/10.1021/acs.iecr.2c03206
Ind. Eng. Chem. Res. 2022, 61, 18744−18761

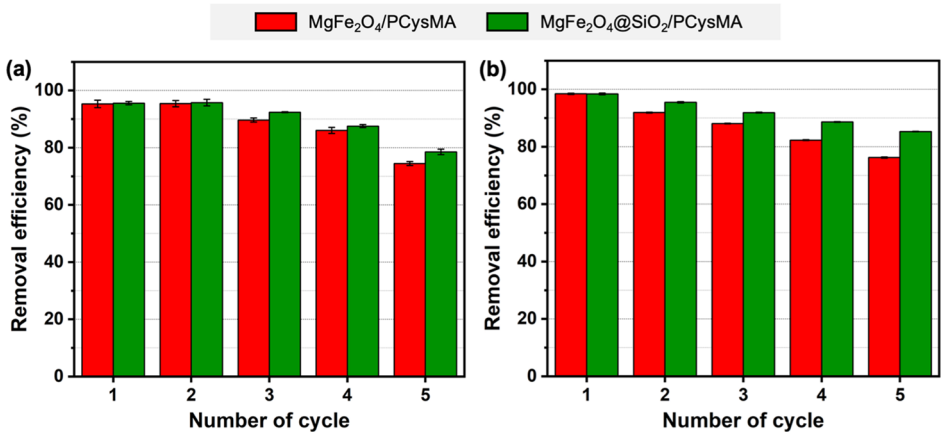

Figure 10. Reusability of $MgFe_2O_4$/PCysMA and $MgFe_2O_4$@SiO_2/PCysMA nanocomposites for the removal of (a) IC at pH ∼2 and (b) MB at pH ∼10.

3.2.3. Adsorption Isotherms. Adsorption isotherm models were used to explain the relationship between adsorption capacity and adsorbate concentration at equilibrium. The adsorption isotherm models were used to predict adsorption behavior. In this work, the Langmuir and Freundlich isotherms were used to study the adsorption of IC and MB by the nanoadsorbents. The Langmuir isotherm describes the monolayer adsorption of the adsorbate on a homogeneous adsorbent surface.[66] However, the Freundlich isotherm describes heterogeneous multilayer adsorption occurring on a solid surface.[54] The linear forms of the Langmuir and Freundlich models are given by eqs 3 and 4, respectively.

$$\frac{C_e}{q_e} = \frac{1}{K_L q_m} + \frac{C_e}{q_m} \tag{3}$$

$$\log\ q_e = \log\ K_F + \frac{1}{n}\ \log C_e \tag{4}$$

where q_e is the amount of dye adsorbed on the adsorbent (mg g^{-1}), C_e is the equilibrium dye concentration (mg L^{-1}), q_m is the maximum adsorption capacity (mg g^{-1}), K_L is the Langmuir constant (L mg^{-1}), and K_F and n are empirical Freundlich constants related to the maximum adsorption capacity.

In the study of pH-selective adsorption, isotherms for the adsorption of IC and MB by $MgFe_2O_4$ and $MgFe_2O_4$@SiO_2 NPs (i.e., pristine and modified NPs) were obtained at pH ∼2 and ∼10, respectively. The linear fits of the Langmuir and Freundlich isotherm models to the adsorption data are given in Figure S9. The calculated parameters obtained from these fitting curves are listed in Table 3. According to the R^2 values obtained for fits with the Langmuir and Freundlich isotherm models, data for the adsorption of IC and MB by all nanoadsorbents were fitted better with the Langmuir isotherm model. This indicated that the adsorption of IC and MB onto the surfaces of the nanoadsorbents resulted in monolayers. Compared to the unmodified nanoadsorbents (i.e., $MgFe_2O_4$ and $MgFe_2O_4$@SiO_2 NPs), the differences in the q_m values of the $MgFe_2O_4$/PCysMA and $MgFe_2O_4$@SiO_2/PCysMA nanoadsorbents for IC were ∼22 and ∼135 mg g^{-1}, respectively (see Table 3). Likewise, the rise in q_m values for these modified nanoadsorbents and MB were ∼48 and ∼128 mg g^{-1}, respectively. These findings indicated that the maximum capacities of the PCysMA-modified nanoadsorbents for the adsorption of IC and MB were significantly enhanced compared to those of the unmodified nanoadsorbents. Even though the S_{BET} and average pore radius of the nanoadsorbents decreased after polymerization with PCysMA (Table 2), the q_m values of PCysMA-modified nanoadsorbents (i.e., $MgFe_2O_4$/PCysMA and $MgFe_2O_4$@SiO_2/PCysMA) for IC and MB increased. The enhancement of IC and MB adsorption could be due to the presence and incremental increase of appropriate active sites originating from PCysMA (i.e., $-NH_2$ and −COOH groups).[67] In addition, the increases in the q_m values of the $MgFe_2O_4$@SiO_2/PCysMA nanoadsorbent for both IC and MB were higher than those of the $MgFe_2O_4$/PCysMA nanoadsorbent. This was attributed to the higher amounts of PCysMA immobilized on the surfaces of the $MgFe_2O_4$@SiO_2 NPs than on those of the $MgFe_2O_4$ NPs, which is consistent with the TGA results (see Section 3.1). The higher amounts of PCysMA on the $MgFe_2O_4$@SiO_2 NPs could be due to the higher amounts of MPS immobilized on their surfaces compared to those of the $MgFe_2O_4$ NPs (see Figure S10). In comparison with the capacities for the adsorption of IC and MB by various magnetic-based adsorbents reported in the literature (see Table S1), the as-synthesized $MgFe_2O_4$/PCysMA and $MgFe_2O_4$@SiO_2/PCysMA nanoadsorbents exhibited higher adsorption capacities for both IC and MB than the prior adsorbents. In addition, the PCysMA-modified nanoadsorbents can remove either IC or MB from aqueous solutions by tailoring the solution pH, suggesting that these nanoadsorbents are attractive materials for the removal of IC and MB.

3.3. Reusability and Stability of the $MgFe_2O_4$/PCysMA and $MgFe_2O_4$@SiO_2/PCysMA Nanocomposites.

To determine the reusability of $MgFe_2O_4$/PCysMA and $MgFe_2O_4$@SiO_2/PCysMA nanoadsorbents for the adsorption of IC and MB, five cycles of adsorption−desorption processes were performed with these dyes, as shown in Figure 10. High efficiencies for the removal of IC (∼90%) by the PCysMA-modified nanoadsorbents were obtained in the first three cycles (see Figure 10a). After the fifth cycle, the efficiencies for the removal of IC had decreased to ∼74 and ∼80% for the $MgFe_2O_4$/PCysMA and $MgFe_2O_4$@SiO_2/PCysMA nanoadsorbents, respectively. For MB adsorption, high efficiencies for removal (∼90%) by both $MgFe_2O_4$/PCysMA and $MgFe_2O_4$@SiO_2/PCysMA nanoadsorbents were obtained in the first three cycles, as with IC adsorption (see Figure 10b). After the fifth

https://doi.org/10.1021/acs.iecr.2c03206
Ind. Eng. Chem. Res. 2022, 61, 18744−18761

cycle, the efficiencies for the removal of MB had decreased to ~76 and ~85% for the $MgFe_2O_4$/PCysMA and $MgFe_2O_4$@SiO_2/PCysMA nanoadsorbents, respectively. The reduction of removal efficiency as a function of the regeneration cycle could be due to (1) a decrease in the number of active sites attributed to incomplete desorption of loaded dyes (Figure S11) and (2) a decrease in the weight of the adsorbent during the adsorption−desorption cycles (Figure S12). Although the PCysMA-modified nanoadsorbents were used for 5 adsorption−desorption cycles, high efficiencies for the adsorption of IC and MB were still obtained. This finding suggested that the PCysMA-modified nanoadsorbents provided excellent reusability for IC and MB adsorption.

To further investigate the stability of the $MgFe_2O_4$ phase in the PCysMA-modified nanoadsorbents during adsorption−desorption processes, XRD patterns were collected for the $MgFe_2O_4$/PCysMA and $MgFe_2O_4$@SiO_2/PCysMA nanoadsorbents before and after adsorption of IC and MB, as shown in Figure S13. The results showed no changes in the diffraction peaks for any of the patterns. This indicated that the $MgFe_2O_4$ phases of the composite nanoadsorbents remained stable during adsorption−desorption of both IC and MB, suggesting the high stabilities of the nanoadsorbents.

4. CONCLUSIONS

In this study, poly(cysteine methacrylate) composited with two types of magnetic nanoparticles (i.e., $MgFe_2O_4$/PCysMA and $MgFe_2O_4$@SiO_2/PCysMA) was synthesized to study pH-selective adsorption of anionic indigo carmine and cationic methylene blue dyes. Before the preparation of the nanocomposites, control studies on pH-dependent adsorption of IC and MB were also performed. Successful syntheses of the $MgFe_2O_4$/PCysMA and $MgFe_2O_4$@SiO_2/PCysMA nanocomposites were confirmed with several characterization techniques, including XRD, FTIR, TGA, ζ potential analyses, VSM, FE-SEM, TEM, N_2 adsorption−desorption, and XPS. The adsorption studies of dyes showed enhanced pH-dependent adsorption of IC and MB by $MgFe_2O_4$ and $MgFe_2O_4$@SiO_2 NPs after grafting with the polymer. Specifically, pH-dependent adsorption of the dyes indicated that the as-synthesized nanocomposites could efficiently adsorb either IC or MB (>90%) by tailoring the initial pH of the solution appropriately (i.e., pH ~2 for IC and pH ~10 for MB). In addition, the nanocomposites exhibited highly pH-selective adsorption of IC and MB from both single and binary dye systems. Interestingly, the $MgFe_2O_4$@SiO_2/PCysMA nanoadsorbent showed higher pH-selective adsorption of IC and MB from binary dye systems compared to the $MgFe_2O_4$/PCysMA nanoadsorbent. With regard to the adsorption isotherms, the maximum capacities for IC and MB adsorption by the $MgFe_2O_4$/PCysMA and $MgFe_2O_4$@SiO_2/PCysMA nanoadsorbents were 94.6 and 50.0 mg g^{-1} and 139.5 and 138.3 mg g^{-1}, respectively. Apart from the pH-selective nanoadsorbents, the nanocomposites showed enhanced capacities for the adsorption of both IC and MB compared to those of the pristine nanoparticles (i.e., $MgFe_2O_4$ and $MgFe_2O_4$@SiO_2 NPs). The highly pH-selective and enhanced capacities of the nanocomposites for the adsorption of the dyes were attributed to the following: (1) the presence of specific functional groups (i.e., $-NH_2$ and $-COOH$), originating from the PCysMA, and (2) the higher amount of grafted polymer for the $MgFe_2O_4$@SiO_2/PCysMA nanocomposite due to the presence of silica. In terms of regeneration, the nanocomposites also exhibited high reusability and stability. On the whole, the $MgFe_2O_4$/PCysMA and $MgFe_2O_4$@SiO_2/PCysMA nanocomposites exhibited several attractive characteristics (i.e., pH-tunable adsorption for dyes, easy magnetic separation, and good reusability). Specifically, the $MgFe_2O_4$@SiO_2/PCysMA nanocomposite is the superior candidate due to its highly pH-selective adsorption and high adsorption capacity, which demonstrate that it is a promising and alternative nanoadsorbent for application in wastewater treatment and sensors.

■ ASSOCIATED CONTENT

Supporting Information

The Supporting Information is available free of charge at https://pubs.acs.org/doi/10.1021/acs.iecr.2c03206.

Preparations of $MgFe_2O_4$ and $MgFe_2O_4$@SiO_2 NPs; ^1H NMR and ^{13}C NMR chemical shifts of the CysMA monomer; dispersion in water for MPS-modified nanoparticles; digital photos of IC, MB, MO, and RhB in single-component solution systems of dyes before and after the adsorption processes; removal efficiencies of MB using 300 mg L^{-1} of initial MB concentration; removal efficiencies of NR; UV−vis spectrum of IC/MB binary solution; relative removal efficiencies of dyes in binary dye systems composed of 500 mg L^{-1} of each dye; Langmuir and Freundlich isotherms of the adsorption of IC and MB; TGA curves of MPS-modified nanoparticles; desorption efficiencies of IC and MB; weight loss of the nanoadsorbents during regeneration cycles; XRD patterns of the nanoadsorbents before and after the adsorption of IC and MB; and adsorption capacities of IC and MB by magnetic-based adsorbents (PDF)

■ AUTHOR INFORMATION

Corresponding Author

Laongnuan Srisombat − *Department of Chemistry, Faculty of Science, Chiang Mai University, Chiang Mai 50200, Thailand; Center of Excellence in Materials Science and Technology, Chiang Mai University, Chiang Mai 50200, Thailand;* orcid.org/0000-0003-3886-2637; Email: laongnuan.sri@cmu.ac.th

Authors

Tanapong Kunakham − *Department of Chemistry, Faculty of Science, Chiang Mai University, Chiang Mai 50200, Thailand;* orcid.org/0000-0003-3239-9872

Supawitch Hoijang − *Department of Chemistry, Faculty of Science, Chiang Mai University, Chiang Mai 50200, Thailand;* orcid.org/0000-0002-0061-5166

Minh Dang Nguyen − *Department of Chemistry and the Texas Center for Superconductivity, University of Houston, Houston, Texas 77204-5003, United States;* orcid.org/0000-0002-2569-8279

Supon Ananta − *Department of Physics and Materials Science, Faculty of Science and Center of Excellence in Materials Science and Technology, Chiang Mai University, Chiang Mai 50200, Thailand;* orcid.org/0000-0002-1478-3590

T. Randall Lee − *Department of Chemistry and the Texas Center for Superconductivity, University of Houston, Houston, Texas 77204-5003, United States;* orcid.org/0000-0001-9584-8861

Complete contact information is available at:
https://pubs.acs.org/10.1021/acs.iecr.2c03206

Notes

The authors declare no competing financial interest.

■ ACKNOWLEDGMENTS

This research was supported by the Program Management Unit for Human Resources & Institutional Development, Research and Innovation, Office of National Higher Education Science Research and Innovation Policy Council (NXPO) [grant number B16F640001]. The authors also acknowledge partial support from Chiang Mai University. T.K. is grateful to the Development and Promotion of Science and Technology Talents (DPST) scholarship for a Master's degree fellowship. T.R.L. is grateful for generous support from the US Air Force Office of Scientific Research (FA9550-20-1-0349; 20RT0302), the Robert A. Welch Foundation (grant no. E-1320), and the Texas Center for Superconductivity at the University of Houston.

■ REFERENCES

(1) Yang, Z.; Zhu, L.; Chen, L. Selective Adsorption and Separation of Dyes from Aqueous Solution by Core-Shell Structured NH_2-Functionalized UiO-66 Magnetic Composites. *J. Colloid Interface Sci.* **2019**, *539*, 76−86.

(2) Liu, W.; Hu, R.; Li, Y.; Huang, Y.; Wang, Y.; Wei, Z.; Yu, E.; Guo, X. Cross-Linking of Poly(dimethylaminoethyl methacrylate) by Phytic Acid: pH-Responsive Adsorbent for High-Efficiency Removal of Cationic and Anionic Dyes. *RSC Adv.* **2020**, *10*, 4232−4242.

(3) Jia, Z.; Li, Z.; Li, S.; Li, Y.; Zhu, R. Adsorption Performance and Mechanism of Methylene Blue on Chemically Activated Carbon Spheres Derived from Hydrothermally-Prepared Poly(vinyl alcohol) Microspheres. *J. Mol. Liq.* **2016**, *220*, 56−62.

(4) Fan, Y.; Liu, H. J.; Zhang, Y.; Chen, Y. Adsorption of Anionic MO or Cationic MB from MO/MB Mixture Using Polyacrylonitrile Fiber Hydrothermally Treated with Hyperbranched Polyethyleneimine. *J. Hazard. Mater.* **2015**, *283*, 321−328.

(5) Zhang, G.; Shi, L.; Zhang, Y.; Wei, D.; Yan, T.; Wei, Q.; Du, B. Aerobic Granular Sludge-Derived Activated Carbon: Mineral Acid Modification and Superior Dye Adsorption Capacity. *RSC Adv.* **2015**, *5*, 25279−25286.

(6) Wang, X.; Jiang, C.; Hou, B.; Wang, Y.; Hao, C.; Wu, J. Carbon Composite Lignin-Based Adsorbents for the Adsorption of Dyes. *Chemosphere* **2018**, *206*, 587−596.

(7) Zhao, X.; Wang, D.; Xiang, C.; Zhang, F.; Liu, L.; Zhou, X.; Zhang, H. Facile Synthesis of Boron Organic Polymers for Efficient Removal and Separation of Methylene Blue, Rhodamine B, and Rhodamine 6G. *ACS Sustainable Chem. Eng.* **2018**, *6*, 16777−16787.

(8) Aragaw, T. A.; Bogale, F. M. Biomass-Based Adsorbents for Removal of Dyes from Wastewater: A Review. *Front. Environ. Sci.* **2021**, *9*, 558−582.

(9) Zhang, J.; Shao, J.; Guo, P.; Huang, Y. A. Simple and Fast Fe_3O_4 Magnetic Nanoparticles-Based Dispersion Solid Phase Extraction of Sudan Dyes from Food and Water Samples Coupled with High-Performance Liquid Chromatography. *Anal. Methods* **2013**, *5*, 2503−2510.

(10) Deng, S.; Xu, H.; Jiang, X.; Yin, J. Poly(vinyl alcohol)(PVA)-Enhanced Hybrid Hydrogels of Hyperbranched Poly(ether amine)-(hPEA) for Selective Adsorption and Separation of Dyes. *Macromolecules* **2013**, *46*, 2399−2406.

(11) Jiang, H. L.; Xu, M. Y.; Xie, Z. W.; Hai, W.; Xie, X. L.; He, F. A. Selective Adsorption of Anionic Dyes from Aqueous Solution by a Novel β-Cyclodextrin-Based Polymer. *J. Mol. Struct.* **2020**, *1203*, 127373.

(12) Mantasha, I.; Saleh, H. A.; Qasem, K. M.; Shahid, M.; Mehtab, M.; Ahmad, M. Efficient and Selective Adsorption and Separation of Methylene Blue (MB) from Mixture of Dyes in Aqueous Environment Employing a Cu (II) Based Metal Organic Framework. *Inorg. Chim. Acta* **2020**, *511*, 119787.

(13) Liu, Y.; Jia, J.; Gao, T.; Wang, X.; Yu, J.; Wu, D.; Li, F. Rapid, Selective Adsorption of Methylene Blue from Aqueous Solution by Durable Nanofibrous Membranes. *J. Chem. Eng. Data* **2020**, *65*, 3998−4008.

(14) Jaseela, P.; Garvasis, J.; Joseph, A. Selective Adsorption of Methylene blue (MB) Dye from Aqueous Mixture of MB and Methyl Orange (MO) Using Mesoporous Titania (TiO_2)-Polyvinyl Alcohol (PVA) Nanocomposite. *J. Mol. Liq.* **2019**, *286*, 110908.

(15) Chatterjee, S.; Guha, N.; Krishnan, S.; Singh, A. K.; Mathur, P.; Rai, D. K. Selective and Recyclable Congo Red Dye Adsorption by Spherical Fe_3O_4 Nanoparticles Functionalized with 1,2,4,5-Benzenetetracarboxylic Acid. *Sci. Rep.* **2020**, *10*, 111.

(16) Sarkar, A. K.; Saha, A.; Panda, A. B.; Pal, S. pH Triggered Superior Selective Adsorption and Separation of Both Cationic and Anionic Dyes and Photocatalytic Activity on a Fully Exfoliated Titanate Layer-Natural Polymer Based Nanocomposite. *Chem. Commun.* **2015**, *51*, 16057−16060.

(17) Biehl, P.; Wiemuth, P.; Lopez, J. G.; Barth, M. C.; Weidner, A.; Dutz, S.; Peneva, K.; Schacher, F. Weak Polyampholytes at the Interface of Magnetic Nanocarriers: a Facile Catch-and-Release Platform for Dyes. *Langmuir* **2020**, *36*, 6095−6105.

(18) Singh, R.; Pal, D.; Mathur, A.; Singh, A.; Krishnan, M. A.; Chattopadhyay, S. An Efficient pH Sensitive Hydrogel, with Biocompatibility and High Reusability for Removal of Methylene Blue Dye from Aqueous Solution. *React. Funct. Polym.* **2019**, *144*, 104346.

(19) Aghaei, E.; Alorro, R. D.; Encila, A. N.; Yoo, K. Magnetic Adsorbents for the Recovery of Precious Metals from Leach Solutions and Wastewater. *Metals* **2017**, *7*, 529−561.

(20) Fu, Q.; Zhang, L.; Zhang, H.; Chen, X.; Li, M.; Gong, M. Ice- and MOF-Templated Porous Carbonaceous Monoliths for Adsorptive Removal of Dyes in Water with Easy Recycling. *Environ. Res.* **2020**, *186*, 109608.

(21) Yadav, P.; Hafeez, S.; Jaishankar, J.; Srivastava, P.; Nebhani, L. Antimicrobial and Responsive Zwitterionic Polymer Based on Cysteine Methacrylate Synthesized via RAFT Polymerization. *Polym. Sci., Ser. A* **2021**, *63*, 505−514.

(22) Mu, L.; Gao, Y.; Hu, X. L-Cysteine A Biocompatible, Breathable and Beneficial Coating for Graphene Oxide. *Biomaterials* **2015**, *52*, 301−311.

(23) Ladmiral, V.; Charlot, A.; Semsarilar, M.; Armes, S. P. Synthesis and Characterization of Poly(amino acid methacrylate)-Stabilized Diblock Copolymer Nano-Objects. *Polym. Chem.* **2015**, *6*, 1805−1816.

(24) Samiey, B.; Cheng, C. H.; Wu, J. Organic-Inorganic Hybrid Polymers as Adsorbents for Removal of Heavy Metal Ions from Solutions: A Review. *Materials* **2014**, *7*, 673−726.

(25) Nonkumwong, J.; Ananta, S.; Srisombat, L. Effective Removal of Lead (II) from Wastewater by Amine-Functionalized Magnesium Ferrite Nanoparticles. *RSC Adv.* **2016**, *6*, 47382−47393.

(26) Nonkumwong, J.; Pakawanit, P.; Wipatanawin, A.; Jantaratana, P.; Ananta, S.; Srisombat, L. Synthesis and Cytotoxicity Study of Magnesium Ferrite-Gold Core-Shell Nanoparticles. *Mater. Sci. Eng. C.* **2016**, *61*, 123−132.

(27) O'Reilly, R. K. Using Controlled Radical Polymerisation Techniques for the Synthesis of Functional Polymers Containing Amino Acid Moieties. *Polym. Int.* **2010**, *59*, 568−573.

(28) Ji, Y.; Lv, R.; Song, S.; Huang, J.; Zhang, L.; Huang, G.; Li, J.; Ou, J. Facile Fabrication of Zwitterionic Magnetic Composites by One-Step Distillation-Precipitation Polymerization for Highly Specific Enrichment of Glycopeptides. *Anal. Chim. Acta* **2019**, *1053*, 43−53.

(29) Zheng, X.; Zheng, H.; Zhou, Y.; Sun, Y.; Zhao, R.; Liu, Y.; Zhang, S. Enhanced Adsorption of Orange G from Aqueous Solutions by Quaternary Ammonium Group-Rich Magnetic Nanoparticles. *Colloids Surf. A* **2019**, *580*, 123746.

(30) Aoopngan, C.; Nonkumwong, J.; Phumying, S.; Promjantuek, W.; Maensiri, S.; Noisa, P.; Pinitsoontorn, S.; Ananta, S.; Srisombat, L. Amine-Functionalized and Hydroxyl-Functionalized Magnesium Ferrite Nanoparticles for Congo Red Adsorption. *ACS Appl. Nano Mater.* **2019**, *2*, 5329−5341.
(31) Hoijang, S.; Wangkarn, S.; Ieamviteevanich, P.; Pinitsoontorn, S.; Ananta, S.; Randall Lee, T. R.; Srisombat, L. Silica-Coated Magnesium Ferrite Nanoadsorbent for Selective Removal of Methylene Blue. *Colloids Surf. A* **2020**, *606*, 125483.
(32) Alswieleh, A. M.; Cheng, N.; Canton, I.; Ustbas, B.; Xue, X.; Ladmiral, V.; Xia, S.; Ducker, R. E.; El Zubir, O.; Cartron, M. L.; Hunter, C. N.; Leggett, G. J.; Armes, S. P. Zwitterionic Poly(amino acid methacrylate) Brushes. *J. Am. Chem. Soc.* **2014**, *136*, 9404−9413.
(33) Yang, J. J.; Huang, Y. C.; Chuang, T. H.; Herr, D. R.; Hsieh, M. F.; Huang, C. J.; Huang, C. M. Cysteine-Capped Hydrogels Incorporating Copper as Effective Antimicrobial Materials Against Methicillin-Resistant Staphylococcus aureus. *Microorganisms* **2020**, *8*, 149.
(34) Chen, Y.; Xiong, Z.; Zhang, L.; Zhao, J.; Zhang, Q.; Peng, L.; Zhang, W.; Ye, M.; Zou, H. Facile Synthesis of Zwitterionic Polymer-Coated Core-Shell Magnetic Nanoparticles for Highly Specific Capture of N-Linked Glycopeptides. *Nanoscale* **2015**, *7*, 3100−3108.
(35) Guo, Z.; Pereira, T.; Choi, O.; Wang, Y.; Hahn, H. T. Surface Functionalized Alumina Nanoparticle Filled Polymeric Nanocomposites with Enhanced Mechanical Properties. *J. Mater. Chem.* **2006**, *16*, 2800−2808.
(36) Karabela, M. M.; Sideridou, I. D. Effect of the Structure of Silane Coupling Agent on Sorption Characteristics of Solvents by Dental Resin-Nanocomposites. *Dent. Mater.* **2008**, *24*, 1631−1639.
(37) Shirzadi, Z.; Baharvand, H.; Nezhati, M. N.; Sajedi, R. H. Synthesis of Nonlinear Polymer Brushes on Magnetic Nanoparticles as an Affinity Adsorbent for His-Tagged Xylanase Purification. *Colloid Polym. Sci.* **2020**, *298*, 1597−1607.
(38) Ge, Y.; Li, Y.; Zu, B.; Zhou, C.; Dou, X. AM-DMC-AMPS Multi-Functionalized Magnetic Nanoparticles for Efficient Purification of Complex Multiphase Water System. *Nanoscale Res. Lett.* **2016**, *11*, 217.
(39) Pang, A. L.; Ismail, H.; Bakar, A. A. Tensile Properties, Water Resistance, and Thermal Properties of Linear Low-Density Polyethylene/Polyvinyl Alcohol/Kenaf Composites: Effect of 3-(Trimethoxysilyl) Propyl Methacrylate (TMS) as a Silane Coupling Agent. *Bioresources* **2016**, *11*, 5889−5904.
(40) Valencia, L.; Kumar, S.; Jalvo, B.; Mautner, A.; Salazar-Alvarez, G.; Mathew, A. P. Fully Bio-Based Zwitterionic Membranes with Superior Antifouling and Antibacterial Properties Prepared via Surface-Initiated Free-Radical Polymerization of Poly(cysteine methacrylate). *J. Mater. Chem. A* **2018**, *6*, 16361−16370.
(41) Parker, S. F. Assignment of the Vibrational Spectrum of L-Cysteine. *Chem. Phys.* **2013**, *424*, 75−79.
(42) Jung, H. S.; Moon, D. S.; Lee, J. K. Quantitative Analysis and Efficient Surface Modification of Silica Nanoparticles. *J. Nanomater.* **2012**, *2012*, 593471.
(43) Kang, D.; Yu, X.; Ge, M.; Song, W. One-Step Fabrication and Characterization of Hierarchical $MgFe_2O_4$ Microspheres and Their Application for Lead Removal. *Microporous Mesoporous Mater.* **2015**, *207*, 170−178.
(44) Zhou, B.; Tang, Y.; Zhao, L.; Guo, L.; Zhou, J. Novel Fe_3O_4-Poly (methacryloxyethyltrimethyl ammonium chloride) Adsorbent for the Ultrafast and Efficient Removal of Anionic Dyes. *RSC Adv.* **2021**, *11*, 1172−1181.
(45) Aliyan, N.; Mirkazemi, S.; Masoudpanah, S.; Akbari, S. The Effect of Post-Calcination on Cation Distributions and Magnetic Properties of the Coprecipitated $MgFe_2O_4$ Nanoparticles. *Appl. Phys. A* **2017**, *123*, 446.
(46) Goswami, B.; Mahanta, D. Polyaniline-Fe_3O_4 and Polypyrrole-Fe_3O_4 Magnetic Nanocomposites for Removal of 2,4-Dichlorophenoxyacetic Acid from Aqueous Medium. *Environ. Chem. Eng.* **2020**, *8*, 103919.
(47) Bagbi, Y.; Sarswat, A.; Mohan, D.; Pandey, A.; Solanki, P. R. Lead and Chromium Adsorption from Water Using L-Cysteine Functionalized Magnetite (Fe_3O_4) Nanoparticles. *Sci. Rep.* **2017**, *7*, 7672.
(48) Mohapatra, J.; Elkins, J.; Xing, M.; Guragain, D.; Mishra, S. R.; Liu, J. P. Magnetic-Field-Induced Self-Assembly of FeCo/$CoFe_2O_4$ Core/Shell Nanoparticles with Tunable Collective Magnetic Properties. *Nanoscale* **2021**, *13*, 4519−4529.
(49) Sezer, N.; Arı, İ.; Biçer, Y.; Koç, M. Superparamagnetic Nanoarchitectures: Multimodal Functionalities and Applications. *J. Magn. Magn. Mater.* **2021**, *538*, 168300.
(50) Pylypchuk, I. V.; Kołodyńska, D.; Kozioł, M.; Gorbyk, P. Gd-DTPA Adsorption on Chitosan/Magnetite Nanocomposites. *Nanoscale Res. Lett.* **2016**, *11*, 168.
(51) Maponya, T. C.; Ramohlola, K. E.; Kera, N. H.; Modibane, K. D.; Maity, A.; Katata-Seru, L. M.; Hato, M. J. Influence of Magnetic Nanoparticles on Modified Polypyrrole/*m*-Phenylediamine for Adsorption of Cr (VI) from Aqueous Solution. *Polymers* **2020**, *12*, 679.
(52) Ossonon, B. D.; Bélanger, D. Synthesis and Characterization of Sulfophenyl-Functionalized Reduced Graphene Oxide Sheets. *RSC Adv.* **2017**, *7*, 27224−27234.
(53) Bushell, M.; Beauchemin, S.; Kunc, F.; Gardner, D.; Ovens, J.; Toll, F.; Kennedy, D.; Nguyen, K.; Vladisavljevic, D.; Rasmussen, P. E.; Johnston, L. J. Characterization of Commercial Metal Oxide Nanomaterials: Crystalline Phase, Particle Size and Specific Surface Area. *Nanomaterials* **2020**, *10*, 1812.
(54) Sarkar, N.; Sahoo, G.; Das, R.; Swain, S. K. Three-Dimensional Rice Straw-Structured Magnetic Nanoclay-Decorated Tripolymeric Nanohydrogels as Superadsorbent of Dye Pollutants. *ACS Appl. Nano Mater.* **2018**, *1*, 1188−1203.
(55) Wang, L.; Li, J.; Wang, Y.; Zhao, L.; Jiang, Q. Adsorption Capability for Congo Red on Nanocrystalline MFe_2O_4 (M = Mn, Fe, Co, Ni) Spinel Ferrites. *Chem. Eng. J.* **2012**, *181-182*, 72−79.
(56) Hoijang, S.; Kunakham, T.; Nonkumwong, J.; Faungnawakij, K.; Ananta, S.; Nimmanpipug, P.; Lee, T. R.; Srisombat, L. Surface Modification of Magnesium Ferrite Nanoparticles for Selective and Sustainable Remediation of Congo Red. *ACS Appl. Nano Mater.* **2021**, *4*, 10244−10256.
(57) Rodriguez, J. A.; Ibarra, I. S.; Miranda, J. M.; Barrado, E.; Santos, E. M. Magnetic Solid Phase Extraction Based on Fullerene and Activated Carbon Adsorbents for Determination of Azo Ddyes in Water Samples by Capillary Electrophoresis. *Anal. Methods* **2016**, *8*, 8466−8473.
(58) Bişgin, A. T.; Sürme, Y.; Uçan, M.; Narin, İ. Solid-Phase Extraction and Spectrophotometric Determination of Allura Red (E129) in Foodstuff, Soft drink, Syrup and Energy Drink Samples: A Comparison Study. *Int. J. Food Sci.* **2016**, *51*, 2367−2375.
(59) Korde, S.; Deshmukh, S.; Tandekar, S.; Jugade, R. Implementation of Response Surface Methodology in Physi-Chemisorption of Indigo Carmine Dye Using Modified Chitosan Composite. *Carbohydr. Polym. Technol. Appl.* **2021**, *2*, 100081.
(60) Wang, B.; Yang, X.; Ma, L.; Zhai, L.; Xuan, J.; Liu, C.; Bai, Z. Ultra-High Efficient pH Induced Selective Removal of Cationic and Anionic Dyes from Complex Coexisted Solution by Novel Amphoteric Biocomposite Microspheres. *Sep. Purif. Technol.* **2020**, *231*, 115922.
(61) Pan, J.; Zhou, L.; Chen, H.; Liu, X.; Hong, C.; Chen, D.; Pan, B. Mechanistically Understanding Adsorption of Methyl Orange, Indigo Carmine, and Methylene Blue onto Ionic/Nonionic Polystyrene Adsorbents. *J. Hazard. Mater.* **2021**, *418*, 126300.
(62) Peltonen, L. Practical Guidelines for the Characterization and Quality Control of Pure Drug Nanoparticles and Nano-Cocrystals in the Pharmaceutical Industry. *Adv. Drug Delivery Rev.* **2018**, *131*, 101−115.
(63) Wang, J.; Chen, W.; Zhang, M.; Zhou, R.; Li, J.; Zhao, W.; Wang, L. Optimize the Preparation of Fe_3O_4-Modified Magnetic Mesoporous Biochar and its Removal of Methyl Orange in Wastewater. *Environ. Monit. Assess.* **2021**, *193*, 179.

https://doi.org/10.1021/acs.iecr.2c03206
Ind. Eng. Chem. Res. 2022, 61, 18744−18761

(64) Mittal, H.; Mishra, S. B. Gum Ghatti and Fe_3O_4 Magnetic Nanoparticles Based Nanocomposites for the Effective Adsorption of Rhodamine B. *Carbohydr. Polym.* **2014**, *101*, 1255−1264.
(65) Chen, K.; Du, L.; Gao, P.; Zheng, J.; Liu, Y.; Lin, H. Super and Selective Adsorption of Cationic Dyes onto Carboxylate-Modified Passion Fruit Peel Biosorbent. *Front. Chem.* **2021**, *9*, 646492.
(66) Khan, A. A.; Kumari, S.; Chowdhury, A.; Hussain, S. Phase Tuned Originated Dual Properties of Cobalt Sulfide Nanostructures as Photocatalyst and Adsorbent for Removal of Dye Pollutants. *ACS Appl. Nano Mater.* **2018**, *1*, 3474−3485.
(67) Saleem, J.; Shahid, U. B.; Hijab, M.; Mackey, H.; McKay, G. Production and Applications of Activated Carbons as Adsorbents from Olive Stones. *Biomass Convers. Biorefin.* **2019**, *9*, 775−802.

https://doi.org/10.1021/acs.iecr.2c03206
Ind. Eng. Chem. Res. 2022, 61, 18744−18761